MAGNETOHYDRODYNAMIC COMPUTATION OF FEEDBACK STABILIZATION OF RESISTIVE-SHELL INSTABILITIES IN THE REVERSED FIELD PINCH

by

Elizabeth Jean Zita

A thesis submitted in partial fulfillment of
the requirements for the degree of

Doctor of Philosophy (Physics)

at the
University of Wisconsin - Madison
1993

MAGNETOHYDRODYNAMIC COMPUTATION OF FEEDBACK STABILIZATION OF RESISTIVE-SHELL INSTABILITIES IN THE REVERSED FIELD PINCH

Elizabeth Jean Zita

under the supervision of Professor Stewart C. Prager

MHD computations demonstrate that feedback can sustain reversal and reduce loop voltage in resistive-shell reversed field pinch (RFP) plasmas. In the absence of a close-fitting conducting shell, feedback with conducting coils on ~2R/a tearing modes resonant near axis is found to restore plasma parameters to nearly their levels with a close-fitting conducting shell. When original dynamo modes are stabilized, neighboring tearing modes grow to maintain the RFP dynamo more efficiently. This suggests that experimentally observed limits on RFP pulselengths to the order of the shell time can be overcome by applying feedback to a few helical modes. Feedback with resistive coils yields information on requirements for more physically realistic feedback systems and on the potentiality of improvement of resistive-shell plasma parameters beyond the conducting-shell case. Plasma response to shell rotation is investigated, and issues relevant to mode locking and feedback rotation of individual modes are discussed.

 Stewart C Prager

ACKNOWLEDGEMENTS

First, I must thank the coauthors of the DEBS code for developing this excellent research tool, from the original author, Dalton Schnack, to Bill Ho, whose version of DEBS I inherited. They not only provided their increasingly sophisticated code, but also shared insights on numerical MHD plasmas and advice on the dirty details of running DEBS on the MFECC → NERSC Crays (a process made especially interesting by endless system software changes). Thanks also to the NERSC consultants for rescuing crashed runs when possible and helping baffled users like me negotiate the shifting terrain of the CTSS, then UNICOS, operating systems.

I am very grateful to Dr. Prager for giving me the chance to try my hand at computational work and for having faith in me (or trying to) when difficulties seemed insurmountable. He helped to define the questions my research would investigate, clarify and sort out confusions, and interpret results intuitively and analytically.

I probably could not have completed this work without the emotional support of many womyn friends and my brothers, Rich and Pete Nilles. Group members at Ada James Campus Womyn's Center and Harmonia gave courage to persevere with their examples and their empathy. Several womyn in the UW physics department offered valuable

support, including Bernice Durand, who generously listened to and critiqued presentations of my work and offered guidance on a spectrum of concerns. Efforts shared with many members of Madison's womyn's community on personal and political issues have been vital for development of a dynamic balance between life and work. Among the loving friends who have laughed and cried with me in Madison, special thanks to Rain Zephyr-mensis for her patience and to Pam Meyer and Stasia Ruskie for their encouragement. Interstellar Scrabble Champ Becky Leidner has been a consistent source of moral support, delight, and wisdom; this thesis is dedicated to her.

TABLE OF CONTENTS

APPENDICES:

CHAPTER 1

INTRODUCTION

1.1 The Reversed Field Pinch

The Reversed Field Pinch (RFP) is a toroidal configuration for magnetic confinement of plasma. The primary long-term goal of RFP research is to demonstrate the feasibility of the RFP's magnetic geometry for confinement and heating of plasma and, ultimately, for generating energy from fusion of plasma ions. With this goal probably decades in the future, shorter term physics goals such as understanding RFP dynamo, heating, and transport processes are currently significant motivators.

In an RFP, the equilibrium plasma current drives a pinching poloidal magnetic field B_θ comparable in size to the toroidal field B_Z needed to stiffen the plasma against perturbations. (Insofar as the plasma is a conducting fluid, it is frozen to the magnetic field lines.[1]) Energy is supplied by inductive drive of toroidal plasma current density J_Z, which creates the plasma's poloidal magnetic field. The toroidal magnetic field is provided initially by an external field set up in the vacuum chamber prior to the plasma discharge. Thereafter B_Z is driven partly by the paramagnetic plasma current and partly by an internal "dynamo" mechanism which converts poloidal to toroidal flux. The toroidal field spontaneously changes direction near the plasma edge (Fig.1.1a),

vanishing at the "reversal layer" r_v; hence the name "Reversed Field Pinch." The reader is referred to reviews of RFP experiments and theory for historical details.[2,3,4,5,6]

The RFP has several attractive features as a possible fusion reactor, including weak magnetic field, high beta, high energy density, and relatively small size and cost, compared to tokamaks. Consider an RFP and a tokamak with the same plasma current and aspect ratio R/a, where R is the major radius of the torus and a is the minor radius of its cross section (Fig.1.1). The Kruskal-Shafranov[7] limit for ideal kinks constrains the safety factor $q(r) \equiv B_Z r / B_\theta R$, or amount of twist in the helical field lines. Tokamaks satisfy the $q \geq 1$ criterion with a large toroidal field $B_Z \geq B_\theta R/r$, at a cost which increases with B^2; substantial bracing against torques exerted by large $\mathbf{J \times B}$ forces on the metal coils and support structures is also required. The RFP operates beyond the Kruskal-Shafranov limit in a small-toroidal field regime, with stability provided by a conducting shell. Confining comparable energy density with smaller magnetic fields gives the RFP inherently higher beta β = plasma pressure/magnetic pressure. In addition, since RFP current levels are not limited to $q \propto 1/J_Z \geq 1$, and since RFP plasma resistance is relatively high, the plasma can be heated ohmically to ignition. Tokamaks must keep J_Z low for ideal stability, and therefore require expensive auxilliary heating by injection of energetic particles or waves.

There are two primary technological disadvantages of the RFP. First, the requirement of a close-fitting conducting shell for stability to

ideal kinks cannot be satisfied over long time scales, and impedes fine-tuning of RFP profiles. Second, the fluctuations which maintain the RFP field configuration also lead to degraded plasma confinement. This thesis addresses both problems and proposes partial solutions for them.

In the following sections, we review the RFP dynamo (Section 1.2), consider requirements for MHD stability of the RFP (Section 1.3.a), and discuss the stabilizing role and limitations of the conducting shell (Section 1.3.b). Then we examine the RFP's second dilemma: in Section 1.4.a, we discuss the destructive nature of tearing modes, and in Section 1.4.b we review the theory that tearing modes provide RFP sustainment. Finally, Section 1.5 provides an overview of potential solutions to these problems, which constitute the body of this thesis.

1.2 Overview of the RFP dynamo

Magnetic fields in Reversed Field Pinch plasmas typically persist for a duration τ_p over an order of magnitude longer than the resistive diffusion time τ_R of the toroidal field B_z. Inductive drive of J_z sustains B_θ as long as volt-seconds are available from the transformer. Without external magnetic field drive, the vacuum B_z established in the chamber prior to ionization of the fill gas will diffuse away (with an e-folding time $\tau_R \equiv a^2\mu/\eta$ in a plasma of resistivity η and length scale a, if there were no confining shell; otherwise with the L/R time of the resistive shell and external circuit. In a perfectly conducting shell, only field gradients will

diffuse away). In the RFP a "dynamo" mechanism changes B_θ into B_z, sustaining the mean toroidal field for $\tau_p > \tau_R$ without external B_z drive, requiring only a small external edge field to maintain reversed B_z(a).

However, a steady-state, axisymmetric reversed-field pinch cannot exist, according to Cowling's theorem.[8] Since cylindrical symmetry means $\frac{\partial}{\partial z} = \frac{\partial}{\partial \theta} = 0$ and equilibrium (or steady state) means $\frac{\partial \mathbf{B}}{\partial t} = 0$, then, conditions for a cylindrically symmetric equilibrium are ($\mathbf{E} = E\hat{z} = constant$) and $\mathbf{E}_\theta = 0$. We assume steady state cylindrical symmetry and define a parameter $\mu = \mu_0 \mathbf{J}\cdot\mathbf{B}/B^2$ proportional to parallel current density. Since the steady state current is purely toroidal($E = E_z = \eta J_z$), dotting E into B yields a simple relation between μ and B_z:

$$\mathbf{E}\cdot\mathbf{B} = E_z \cdot B_z = \eta\mu B^2 \qquad (1)$$

The poloidal component of Ampere's law $\nabla\times\mathbf{B} = \mu_0\mathbf{J} = \mu\mathbf{B}$ yields a simple relation between μ and gradients in B_z:

$$-\partial \mathbf{B}_z / \partial r = \mu \mathbf{B}_\theta. \qquad (2)$$

Since B_θ is positive throughtout the RFP, (1) and (2) yield the requirement that $\mathrm{sign}(B_z) = -\mathrm{sign}\left(\frac{\partial B_z}{\partial r}\right)$. This condition does not hold in the RFP edge, therefore the assumptions of an axisymmetric steady state are invalid.

Helical fluctuations break the RFP's axisymmetry, permitting a reversed steady state despite Cowling's theorem. The likelihood that the dominant helical fluctuations also provide the RFP dynamo is reviewed

in Section 1.4. It appears that the m=1 helical fluctuations are necessary for the existence (Cowling's theorem) and the sustainment (dynamo) of the RFP.

The RFP dynamo is a cyclic process of fast generation of toroidal flux Φ_Z embedded in the continual slow incomplete resistive diffusion of B_Z. The dynamo is evident experimentally in periodically enhanced toroidal flux on axis and deepened reversal near the edge. Between such "flux jumps" (which are discussed at greater length in Section 1.4.c), Φ_Z and F exhibit their usual slow resistive decay. The net effect of the dynamo is to sustain the plasma in an edge-reversed state.

Faraday's law $\int \mathbf{E}\cdot\mathbf{dl} = -\frac{\partial}{\partial t}\int \mathbf{B}\cdot\mathbf{dA}$ underlies the RFP dynamo[9] process: a negative poloidal electric field at a radius r generates a positive toroidal magnetic flux $\Phi_Z = \int \mathbf{B_z}\cdot\mathbf{dA}$ inside r. A flux-conserving shell at the plasma edge requires a decrease in Φ_Z outside r. Fluctuations in velocity and magnetic field drive the RFP dynamo by creating a negative poloidal electric field (in the fluid frame) near the plasma edge[10,11,12] from Ohm's law, $\mathbf{E}=\eta\mathbf{J}-\mathbf{V}\times\mathbf{B}$. Small scale fluctuations in the parallel cross-product term, $E_F = -<\mathbf{v}\times\mathbf{b}>\cdot\mathbf{B}/|\mathbf{B}|$, can yield a nonzero mean field (Appendix.1).[13] (Here, **v** and **b** are velocity and magnetic field fluctuations, and < > is a sum over toroidal and poloidal mode numbers in Fourier space, equivalent to an ensemble average over the poloidal and toroidal directions in configuration space). Since edge **B** is primarily poloidal in the RFP, the fluctuation-induced E_F is primarily poloidal in

the edge region. Negative poloidal E_F near the reversal surface at $r=r_V$ sustains core B_Z against diffusion. Insofar as the shell conserves flux, $(E_F)_\theta$ also generates negative flux outside r_V, which can reverse edge B_Z. Note that negative $(E_F)_\theta$ at the reversal surface drives the dynamo most efficiently: if negative $(E_F)_\theta$ extends inside r_V, it sustains less axial B_Z; if negative $(E_F)_\theta$ extends outside r_V, it drives less reversed B_Z.

1.3 RFP stability and the role of the conducting shell

This section reviews some of the RFP's stability requirements. Shear and edge field reversal are required for stability to pressure-driven modes. A close-fitting conducting shell is required for stability to kink modes and bulk shifts in the plasma column. The conducting-shell requirement is problematic; proposed solutions are sketched.

1.3.a Stability requirements; Taylor's equilibrium

RFP stability questions can largely be addressed in cylindrical geometry, since small toroidicity is a consequence of comparable B_Z and B_θ levels. In the limit of large aspect ratio R/a or small toroidicity, the RFP plasma is approximated as cylindrical: the toroidal field B_Z becomes the axial field and the poloidal field B_θ becomes the azimuthal field. The axial field helps to stabilize against kink modes, or twisting of the plasma column. Compression of B_Z (via compression by B_θ of the plasma to

which the field is nearly frozen) provides a restoring force against uniform axisymmetric expansions for equilibrium against plasma pressure. (The contribution of a conducting shell to equilibrium and stabilty is considered in section 1.3.b.)

B_θ also shears the field lines, that is, changes their direction from one magnetic flux surface to the next . This stabilizes the RFP against pressure-gradient driven modes. The Suydam[14] criterion for stability against pressure-gradient driven modes

$$\frac{r}{4}\left|\frac{\nabla q}{q}\right|^2 + \frac{2\mu_0 \nabla P}{B_z^2} > 0$$

depends on the safety factor q, which is proportional to the pitch of the helical magnetic field lines, and the shear ($-r^2\nabla q/q^2R$, where $\nabla q = dq/dr$), which quantifies the change in pitch from one magnetic surface to the next. The RFP field lines yield a monotonically decreasing q(r) which reverses sign near the plasma edge (Fig.1.2.a). The Suydam criterion can be violated if a pitch minimum arises (Fig.1.2.b), since this provides a region where $\nabla q = 0$. A pitch minimum permits destabilization by the negative pressure gradient ∇P. In addition, linearly unstable double tearing modes can grow, since a pitch minimum provides two resonant radii for some modes of helicity m/n.[15] (The poloidal mode number = m and toroidal mode number = n.) The RFP's monotonically decreasing safety factor profile consistent with edge field reversal eliminates the danger of a pitch minimum, while providing strong shear stabilization.

Shear stabilization can be envisioned as somewhat analagous to a woven basket holding water: the magnetic field lines serve as the strands of the basket. If all the field lines (strands) were parallel, the plasma (water) could slip through them (e.g. with a Raleigh-Taylor instability). An adjacent layer of crossed lines impedes the flow of the fluid. Nested magnetic flux surfaces with field lines at angles to each other confine the fluid yet more effectively. (The analogy is insufficient in at least two ways: the field lines tend to be only crossed, not woven; and the field lines exert an elastic restoring force when bent.)

The RFP's comparative stability is largely due to its proximity to a minimum energy state, or stable equilibrium, of cylindrical plasmas. The RFP equilibrium is nearly a force-free configuration ($\mathbf{J}\times\mathbf{B}=0$), that is, the plasma current is everywhere nearly parallel to the magnetic field[1]. Lüst and Schlüter describe such systems by $\nabla\times\mathbf{B}=\mu\mathbf{B}$, where $\mu = \mu_0\mathbf{J}\cdot\mathbf{B}/B^2$, generally varies with minor radius. In a perfectly conducting plasma, magnetic fluctuations must satisfy $\partial\mathbf{B}/\partial t - \nabla\times(\mathbf{v}\times\mathbf{B}) = 0$, which describes fluid frozen to field lines. Woltjer shows that this condition together with $\mathbf{B}=\nabla\times\mathbf{A}$ implies the invariance of magnetic helicity $K = \int_{\text{volume}} \mathbf{A}\cdot\mathbf{B}\,dv$ bounded by any flux surface.[16] In a slightly resistive plasma, flux surfaces tear and reconnect and helicity K is probably conserved only as a volume averaged quantity.[17] Assuming constant toroidal flux $\Phi_z = \pi a^2\langle B_z\rangle$ and total helicity <K>, the state of minimum magnetic energy is found to be a force-free configuration with constant μ.[16] The equation $\nabla\times\mathbf{B}=\mu\mathbf{B}$ with constant μ has Bessel function solutions: $B_Z(r)=B_0J_0(\mu r)$ and

$B_\theta(r)=B_0J_1(\mu r)$[18] . Taylor notes that eigenstates with Bessel function magnetic field profiles closely approximate those of the RFP.

Near this minimum energy state there is little free energy available to drive ideal instabilities. The natural relaxation of high-current density toroidal plasmas toward something like the "Taylor state" reveals the RFP as a preferred magnetic geometry for toroidal plasmas. The RFP evolves along a locus of pinch parameter $\Theta = B_\theta(a)/\langle B_z\rangle = \mu_0 J_z a / 2\Phi_z$ and reversal parameter $F = B_z(a)/\langle B_z\rangle$ points slightly displaced from the locus of Taylor state F/Θ points. This is consistent with the experimental deviation from $\mu(r)$=constant: since edge current vanishes, $\mu(r)$ drops smoothly to zero at r=a.[19] In another divergence from the theory, experiments[20,21] and simulations such as those presented in this thesis consistently find dominant helical modes (m=1,n≥2R/a) of slightly shorter wavelength than Taylor's prediction (m=1, n=1.25R/a). This may reflect the existence of a fixed point in the RFP state space toward which the relaxed state is attracted.[22]

1.3.b Role of the conducting shell

One disadvantage of the RFP configuration is its requirement for a close-fitting conducting shell. Both experiment[23,24,25,26] and theory[27,28,29] suggest that the stabilizing influence of the shell is necessary. With a close-fiting conducting shell, MHD fluctuations saturate and the discharge duration time is limited only by the available volt-

seconds driving the plasma current. With a resistive or distant shell, magnetic fluctuations grow well above their conducting-shell amplitudes, with an accompanying increase in the toroidal loop voltage. It has been observed in experiments and MHD computations[30,31] that growing resistive shell modes destroy RFP reversal on the order of the shell time τ_s for soak-in of a magnetic field. (The OHTE experiment appeared to be an exception[32] to this rule; however, OHTE's thick copper helical coils increase the effective shell time to the order of the plasma discharge duration time, in keeping with other experiments.) This presents a fundamental problem, since the stabilizing role of any shell with finite conductivity will vanish on the long time-scale of a steady-state reactor.

A conducting shell provides partial equilibrium control since displacements in the plasma current column induce eddy currents in the shell; these exert a JxB restoring force that tends to push the plasma radially inward, away from the walls. However, the presence of a conducting shell also complicates fine control of the equilibrium position: a vertical magnetic field (providing a horizontal JxB force to center the plasma column) must be able to soak through metal shells enclosing the plasma on the order of the plasma discharge timescale. Therefore these shells must not be too highly conducting. Active equilibrium control more completely centers the plasma column in the vacuum chamber by responding to bulk radial shifts, on a fast timescale compared to the discharge duration time, with externally imposed vertical (horizontal) B fields to center the plasma horizontally (vertically). Optimized

equilibrium control minimizes plasma-wall interactions. Plasma-wall interactions increase high-Z (atomic number) impurities and therefore increase Spitzer (particle collisionality) resistivity $\eta_S \propto Z$. Helicity scrape-off due to flux lines intersecting the vacuum chamber (or limiters) increases the "non-Spitzer" part of the resistivity[33] which can dominate total plasma resistivity. The lower-impedance plasmas demonstrated with active equilibrium control require less loop voltage (V_L) for induction of plasma current[34], and are more reproducible than RFPs with nonideal boundary conditions without active plasma current column centering.

Replacement of a conducting wall with a resistive shell, however, provides additional free energy for growth of ideal instabilities, which may have resonant surfaces in the plasma or in the surrounding vacuum region.[28] At the values of magnetic Lundquist number $S \propto 1/\eta$ used in our computations, these ideal modes grow more slowly and perturb the RFP less than do the dominant resistive modes. Continued numerical investigations into regimes of lower resistivity/higher S are providing[35] more complete characterization of the relative importance of ideal modes in resistive shell RFPs.

To summarize the conducting shell problem: equilibrium control requires a resistive shell (shell time $\tau_S < \tau_p$ plasma discharge duration time) but linearly unstable ideal modes and nonlinearly unstable resistive modes necessitate a close-fitting conducting shell ($\tau_S > \tau_p$).

Several solutions to the conducting shell problem in RFPs have been proposed.[36,37] Initial MHD computational tests of helicity injection suggest that this method of parallel current drive can effectively suppress tearing mode instabilities, but at a high power cost.[38] Ongoing detailed tests seek more efficient helicity injection configurations.[39] This thesis investigates another means of suppression of tearing modes: indirect drive of parallel current through application of edge magnetic fields designed to suppress tearing modes. Results presented here suggest that edge feedback may be a feasible solution to the conducting shell problem, especially at small aspect ratio.

1.4 Resistive tearing modes and the RFP dynamo

1.4.a Resistive tearing modes as instabilities

RFP equilibrium (m,n)=(0,0) profiles are modified primarily by m=1 resistive tearing modes driven by current gradients.[40] The longest wavelength fluctuations resonate on axis; these tend to be largest in amplitude, with significant radial separation between resonant surfaces for tearing modes, though even central modes overlap to some extent. Since nonlinear mode coupling and quasilinear profile modifications are key to RFP dynamics, nonlinear calculations will be necessary to model RFP evolution.[41] The resonant surface for a tearing mode (m,n) lies at the radius r_S where the safety factor $q(r_S) = m/|n|$. At r_S the (m,n) mode has the same pitch as the local magnetic field: the fluctuation amplitude is

constant along the field line, so the mode's wavenumber parallel to the field vanishes ($\mathbf{k}\cdot\mathbf{B}=0$). At this surface, $B(r_S)=0$ in the frame of the perturbation, and field lines can tear and reconnect into magnetic islands and a tearing mode instablity can grow at the resonant surface. With nonzero resistivity the magnetic restoring force for perturbations becomes finite (see App.2):

$$\mathbf{F} = \mathbf{J}\times\mathbf{B} = (\mathbf{v}\times\mathbf{B})\times\mathbf{B} / \eta \approx -\mathbf{v}B^2 / \eta$$

The magnetic field lines can decouple from the plasma fluid, tear across the resonant magnetic flux surface, and reconnect into magnetic islands. Shorter wavelength ($m\geq 2$) modes are linearly stable.[41]

When $R/a=2.5$ and $q\sim 0.2$ at $r=0$, the internal helical fluctuations with $|n| = 5$, 6, or 7 tend to dominate the $m=1$ energy spectra. Internal $m=1$ modes with $|n| > 8$ remain small because their resonant surfaces are crowded close to neighbors' resonant surfaces: the closely-packed modes interact and tear each others' boundary layers before they have a chance to grow to large amplitude. Relative amplitudes of fluctuations are determined by interactions such as $(1,-5)+(0,2) \rightarrow (1,-7)+(1,-3)$. Modes with longer toroidal structures than (1,-4) remain small since $q(0)$ is too low for inclusion of their resonant surfaces in the plasma. The $m=0$ and $m=2$ products of such nonlinear interactions such as $(1,-5) + (1,-6) \rightarrow (2,-11)$ and (0,1) tend to be at least an order of magnitude smaller than the $m=1$ modes, at least in MHD computations with $S=6000$; these may be larger at higher S, where greater turbulence leads to more nonlinear interactions.

The (0,1) can contribute to $m=1$ generation, playing an intermediary role in the dynamo process discussed below, by facilitating cascade of magnetic energy to short-wavelength modes during the transport phase of the dynamo cycle (discussed in Section 1.4.c). These dynamics are supported by bispectral analyses of experimentally measured $\tilde{B}$ fluctuations[42] and power flow analyses of computations.[43] Small-scale $m=2$ modes contribute little to the equilibrium evolution, serving as an energy sink and a medium for further mode-spectrum broadening.[44]

1.4.b Resistive tearing modes as dynamo modes

Several theories have been proposed to explain the RFP dynamo. Kinetic dynamo theory[45] proposes that Φ_Z is produced by fast edge electrons which arise from transport along stochastic field lines. This theory is not self-consistent. Magnetohydrodynamic (MHD) dynamo theories are the most highly developed and most self-consistent explanations for RFP sustainment. In these theories (and in this thesis), "dynamo modes" are by definition those supplying the bulk of negative E_F (that is, directed opposite to the poloidal magnetic field) around the reversal region, as discussed in Section 1.2. Φ_Z production is attributed to $m=0$ modes [46,47] or $m=1$ modes[48,9,12], depending on the RFP's proximity[49] to the Taylor state, where μ=constant (therefore edge current is nonzero). RFPs modeled with the more realistic constraint of zero edge plasma current consistently exhibit $m=1$ dynamo drive and $m=0$ antidynamo[48] (or

degradation instead of sustainment of toroidal flux). That is, when $\mu(a)=0$, the m=0 modes give rise to positive E_F, opposing the dynamo field, while a few m=1 modes drive a strong negative E_F around the reversal surface.

The internally resonant tearing modes responsible for the dynamo sustainment of the RFP are also the dominant RFP fluctuations (with either a conducting or resistive shell)[12]. A small number (approximately equal to the aspect ratio, R/a) of these helical fluctuations are at least an order of magnitude larger than all other fluctuations. They are global in spatial structure, with poloidal and toroidal mode numbers m=1, $|n| \geq 2R/a$. Typically, all internally resonant m=1 modes with $2R/a \leq |n| \leq 3R/a$ are possible dynamo modes.[50]

In fact, edge E_F from m=1 tearing modes resonant near the core provide the RFP dynamo.[48] The m=1 dynamo modes resonate with large amplitude near the axis and drop off toward r=a. They convert poloidal field into mean toroidal field (B_Z) and provide edge reversal of B_Z by driving parallel current near the plasma edge via the fluctuation-induced electric field $E_F=-\langle \mathbf{v}\times\mathbf{b}\rangle\cdot\mathbf{B}/|\mathbf{B}|$. Dynamo modes have positive $E_F(m,n)$ in the core, and negative $E_F(m,n)$ at the edge, changing sign near the modal resonant surface. In the plasma edge or reversal region, E_F provides the dynamo field which sustains toroidal flux inside r_V. In sustaining and reversing B_Z they also contribute to the RFP's ideal stability by enhancing shear without an edge pitch minimum.

In the plasma core, however, the direction of the fluctuation-induced field is opposed to the applied electric field. Therefore growing dynamo modes also suppress $\eta J_{||} = E_{||} - E_F$, or, equivalently, necessitate a higher toroidal loop voltage to sustain the current. While a finite $E_F(0)$ helps suppress the current-driven thermal instability believed to initiate sawteeth, high $E_F(0)$ increases input power costs by increasing loop voltage. One of the goals of our feedback schemes is to reduce the amplitude of the dominant m=1 modes without loss of dynamo.

1.4.c Review of dynamo details

An RFP dynamo is inferred from observations of unusually long plasma discharge duration times. Experimentalists sometimes observe discrete dynamo events in RFPs relatively far from the Taylor state[51]. Excursions from the minimum energy state, e.g. at high Θ and/or large negative F appear in some experiments as "sawteeth" or "flux jumps", which simultaneously increase mean Φ_Z and deepen reversal dramatically. Relaxations toward a lower energy state follow periods of growth to higher magnetic energies. Sawteeth give experimentalists a peek at dynamo processes in the RFP core, since these large excursions from a relaxed state show up even on edge diagnostics. Before a flux jump, m=1 fluctuation activity increases. During a flux jump (a sudden "crash" toward a lower-energy state) the mean toroidal magnetic m=0 flux increases and reversal deepens, profiles flatten, fluctuations quiet down,

and the plasma heats up.[52] Charge exchange analyzers detect a hot ion burst at the plasma edge, and soft x-ray signals indicate hot electrons within the plasma.[53,54] After a flux jump, B_Z and F resume their slow decay, until m=1 precursors signal the beginning of a new cycle.

Consider a peaking in the current density profile $J_Z(r)$ before a flux jump as the starting point of the dynamo cycle. Two main processes contribute to $J_Z(r)$ peaking during the diffusion phase before a sawtooth crash: a global thermal instability, and a circuit response to tearing mode fluctuations. The thermal instability[9] arises because current flows more easily in the hot, conductive core than the cold edge of the RFP, ohmically heating the core further. Resistivity $\eta \propto T^{-3/2}$ drops as the core temperature rises, facilitating increased plasma current in the central region. Meanwhile, the resistive plasma edge remains cool, with $J(a) \approx 0$. Peaked J_Z leads to current profile steepening, and increased gradients in J_Z provide free energy[55] to destabilize axially resonant m=1 tearing modes.

Numerical simulations have illuminated details of the tearing modes' contribution to the dynamo process.[37] Magnetic reconnections increase the flux in internal modes $(m, |n|) \geq (1, 2R/a)$, and their magnetic energies $w_m(m,n) = \frac{1}{2} \int_{volume} b^2(m,n) d\tau$ grow on a resistive diffusion timescale (typically milliseconds). Growing m=1 helical fluctuations twist B_θ into B_Z, enhancing B_Z non-axisymmetrically. (Increased fluctuation activity may also contribute to core plasma heating as the RFP moves further from the Taylor state.[54]) As higher fluctuations demand increased applied

electric field to sustain J_Z at a specified level, and increased E_Z preferentially drives axial current, the net result is increased current density gradients, which exacerbate the tearing mode instability.

Moving further from a stable equilibrium, these dynamics become insupportable. The RFP "crashes" toward a minimum energy state on the hybrid tearing mode timescale $\tau = \tau_R^{3/5} \tau_A^{2/5}$ (between microseconds and milliseconds)[56,40,57]. Toroidal flux generated in m=1 modes becomes m=0 toroidal flux as the tearing modes break flux surfaces. The broken flux surfaces of the helical modes stochasticize field lines, which transport heat and current radially outward. Energy cascades radially outward to smaller-scale modes, broadening the spectra of modal energies.[44] Nonlinear interactions between overlapping tearing modes flatten J_Z as they symmetrize the dynamo-generated $\Phi_Z(1, |n| \geq 2R/a)$ into mean $\Phi_Z(0,0)$. This shows up in a burst of $+B_Z(0,0)$ inside r_V and $-B_Z(0,0)$ outside r_V, sustaining the mean field and deepening reversal. Therefore, in the sawtooth crash, F deepens as W_m/K drops,[12] where the magnetic energy W_m is a sum of $w_m(m,n)$ over all fluctuations and the helicity $K = \int_{volume} \mathbf{A} \cdot \mathbf{B} d\tau$. Without driving current gradients, m=1 fluctuations become quiescent and islands narrow. As J(r) flattens, the peaked J(0) drops and q(0) increases. The higher axial safety factor allows the re-inclusion of low-n resonant fluctuations. Axial tearing modes resume their growth and the cycle repeats.

At low Θ and/or shallow reversal, a bath of small fluctuations interact in a quasi-steady state and drive the dynamo continuously. Fluctuations may not grow large enough to push the RFP far from a minimum energy state. There is less free energy available to drive current gradients so profile peaking and the subsequent flattening "crash" is not dramatic enough to show up on edge diagnostics. Very small flux jumps may be observed in experiments, or edge $\tilde{B}$ coils may report quite smooth B_Z sustainment without discernable flux jumps. In such cases the dynamo cycles gently deep within the RFP, generating helical field near axis and quasilinearly transforming it to axisymmetric B_z near the reversal surface without notably perturbing the plasma edge. Good edge confinement persists and wall interactions remain relatively low. These quiescent, sawtooth-free RFPs have relatively low Z therefore low Spitzer resistivity $\eta_S \propto Z$; low flux scrapeoff[33,58] therefore low anomalous resistivity; and low amplitude m=1 kinking, therefore low inductance; the net result is low input power requirements for a high-quality RFP. Power flow analyses suggest that quasilinear interactions provide the quiescent dynamo while nonlinear interactions in the presence of large m=0 modes drive a sawtoothing dynamo.[43]

1.5 Overview of present research

This work uses MHD computation to examine the feasibility, from a physics perspective, of a feedback solution to the resistive shell problem.

Restoration of helical mode amplitudes and loop voltage to the conducting shell levels would constitute a solution. Reduction of mode amplitudes and V_L below conducting shell levels would be even better. Feedback schemes are devised to sustain the reversed-field configuration in the absence of a conducting shell. We investigate edge feedback suppression of resistive-shell tearing fluctuations as a means of restoring mode amplitudes and V_L to conducting-shell levels, without suppressing the dynamo. We find that effective feedback must not only maintain negative edge E_F of dominant fluctuations, but should also inhibit central E_F. Therefore, an efficient dynamo mode has low positive E_F in the core in addition to negative $E_F(m,n)$ in the outer region. As means towards more efficient RFP sustainment are uncovered, the physics behind dynamo and transport processes is clarified a bit further.

In these tests, the conducting shell is replaced by helical coils which hold the radial magnetic field to specified levels at the plasma boundary, for a few specific helical modes. These boundary conditions for targeted helical modes are easily implemented in the nonlinear, pseudospectral DEBS code.[59] There has been a limited experimental test of feedback of a single mode[34] which agrees well with these numerical tests. In addition, circuits have been examined for related feedback schemes to address engineering feasibility questions.[60,61]

The results of several feedback boundary conditions imposed in the absence of a close-fitting conducting shell are described in this thesis. Our central results appear in Chapter 3, where modal radial fields are nulled at

the plasma edge. This models application of conducting wall boundary conditions only to specified modes, via resonant helical feedback coils. When the few dominant tearing modes are targeted for feedback stabilization, fluctuation levels and V_L approach the low values of the conducting shell case. Chapter 4 investigates $B_r(m,n)|_{a\neq 0}$ feedback schemes, including attempts to suppress mode amplitudes below their levels in the conducting shell. In Ch.4.2, the resistivity of helical feedback coils is varied to determine requirements for a more physically realistic feedback system. In Ch.4.3, coil currents are varied in response to the magnetic fluctuation amplitude at a mode's resonant surface to keep the driving current gradients small. Parameters are found with which these resistive feedback coils can effect an approach to conducting shell plasma parameters. Ch.4.4 notes a resistive-coil scheme which responds to $B_r(a)$.[62] Since experiments have shown improved plasma parameters when a plasma or its islands rotate, we also have begun investigating the effects of rotation and angular acceleration on RFP stability. In Ch.5, fast rotation or rapid spin-up of the bulk plasma is found to approach the conducting shell case, and rotation of individual modes is discussed.

Fig.1.a

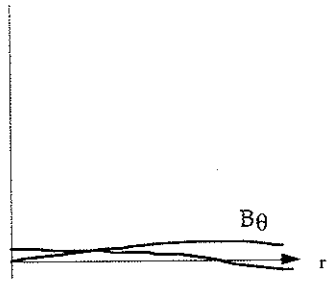

Fig.1.b

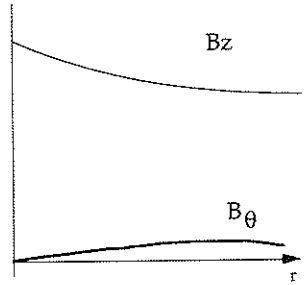

Figure 1.1 Magnetic field profiles for (a) Reversed Field Pinch (RFP) and (b)Tokamak configurations with comparable plasma current

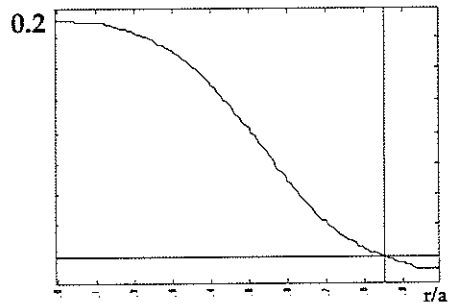

(a)

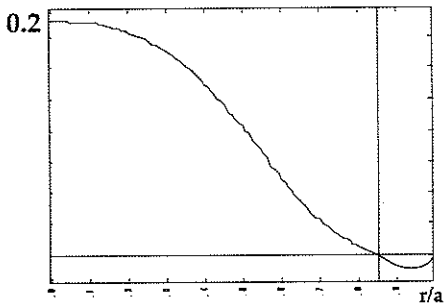

(b)

Fig.1.2 Safety factor $q(r) \equiv B_Z r / B_\theta R$ versus radius ("q profile") for (a) typical RFP, with reversal layer marked by vertical line near edge (b) unstable RFP with pitch minimum in reversal region

References

1 R.Lüst and A.Schlüter, "Kraftfreie Magnetfelder," Z. Astrophys., **34** (1954) 263-282

2 H.A. Bodin, A.A. Newton, Nucl.Fusion **20** (1985) 1255

3 H.A. Bodin, R.A.Krakowski, S.Ortolani, Fusion Technology (1986)

4 K.L.Sidikman, PhD Thesis, University of Wisconsin-Madison, DOE/ER/53212-157 (1990)

5 C.W. Spragins, PhD Thesis, University of Wisconsin-Madison, DOE/ER/ 53198-196 (1992)

6 P.Kirby, Phys.Fluids **31** (1988) 625

7 V.D.Shafranov, Sov.J.At.Energy **1** (1956) 709

MD Kruskal and RM Kulsrud, Phys.Fluids **1** (1958) 265

8 T.G. Cowling, Mon. Not. Roy. Astr. Soc. **94** (1934) 39

9 E.J. Caramana, R.A. Nebel, D.D. Schnack, Phys. Fluids **26** (1983) 1305

10 C.G. Gimblett and M.L. Watkins, *Pulsed High-Beta Plasmas*, Proc. 3rd Top. Conf. on High-Beta Plasmas, Pergamon Press (1976)

11 M.J. Schaffer, Phys. Fluids **27** (1984) 2129

12 D.D. Schnack, E.J. Caramana, R A Nebel, Phys. Fluids **28** (1985), 321

13 H.K. Moffatt, Magnetic Field Generation in Electrically Conducting Fluids, Cambridge University Press (1978)

14 B. Suydam , Proc. 2d International Conference on Peaceful Uses of Atomic Energy **31** (1957) 157

15 D. D. Schnack, PhD Thesis, University of California/ Livermore, Lawrence Livermore Laboratory publication UCRL-52399, 1978

16 L. Woltjer, Proc. Nat. Acad. Sci. **44** (1958) 489

17 J.B. Taylor, Phys. Rev. Lett. **33** (1974) 1139

18 S. Chandrasekhar, Proc. Nat. Acad. Sci.42 (1956) 1-5

19 W. Shen, J.C. Sprott, Phys. Fluids **B** (1991) 1225

20 R.J. LaHaye, P.S.C. Lee, M.J. Schaffer, T. Tamano, P.L. Taylor, Nucl.Fusion **28** (1988) 918

21 A. Almagri, S. Assadi, J. Beckstead, et al., *Edge Fluctuations in the MST Reversed Field Pinch*, in Physics of Alternative Magnetic Confinement Schemes, S. Ortolani and E. Sindoni, Eds., Societa Italiana di Fisica, (1991) 223

22 S. Cappello and R. Paccagnella, Phys.Fluids B **4** (1992) 611

23 T. Tamano, W.D. Bard, T.Carlstrom, C.Chu, R.R.Goforth, Y.Kondoh, R.J.La Haye, P.Lee, E.J.Nilles, M.T.Saito, M.J.Schaffer, P.L.Taylor, Plasma Phys. and Controlled Nuclear Fusion Res. (Proc. 11th Int. Conf. Kyoto, 1986), Vol.2, IAEA, Vienna (1987) 655

24 B. Alper, M.K. Bevir, H.A.B. Bodin, C.A. Bunting, P.G. Carolan, J. Cunnane, D.E. Evans, C.G. Gimblett, R.J. Hayden, T.C. Hender, A. Lazaros, R.W. Moses, A.A. Newton, P.G. Noonan, R. Paccagnella, A. Patel, H.Y.W. Tsui, P.D. Wilcock, Plasma Phys. Controlled Fusion **31** (1989) 205

25 P. Greene, G. Barrick, S. Robertson, Phys. Fluids B **2** (1990) 3059

26 S. Masamune, US-Japan RFP Workshop on Anomalous Ion Heating and Related Topics University of Wisconsin, Madison, Wisconsin (2-4 March 1992)

27 D.C. Robinson, Plasma Phys.13 (1971) 439

28 Y.L. Ho and S.C.Prager, Phys. Fluids B **3** (1991) 3099

29 C.G. Gimblett and D.D. Schnack, *Simulation of the thin shell and secondary shell HBTX1C experiments*, Science Applications International Corporation SAIC-91/1016:APPAT-140 (1991)

30 Y.L. Ho, S.C. Prager, D.D. Schnack, Phys.Rev.Lett.**62** (1989) 1504

31 E.J. Nilles, S.C. Prager, Y.L. Ho, Bull. Am. Phys. Soc. **34** (1989) 2147

32 R.R. Goforth, T.N. Carlstrom, C. Chu, B. Curwen, D. Graumann, P.S.C. Lee. E.J. Nilles, T. Ohkawa, M.J. Schaffer, T. Tamano, P.L. Taylor, T.S. Taylor, Nucl. Fusion **26** (1986) 515

33 T.R. Jarboe and B. Alper, Phys. Fluids **30** (1987) 1177

34 B. Alper, M.K. Bevir, H.A.B. Bodin, C.A. Bunting, P.G. Carolan, J.A. Cunnane, D.E. Evans, C.G. Gimblett, R.J. La Haye, P. Martin, A.A. Newton, P.G. Noonan, A. Patel, S. Robertson, H.Y.W. Tsui, P.D. Wilcock, *Results from HBTX reversed field pinch with close and distant resistive shells*, in Controlled Fusion and Plasma Physics (Proc.16th Eur. Conf. Venice, 1989), Vol. 13B , Part II, European Physical Society (1989)

35 D.D. Schnack and S. Ortolani, Nuclear Fusion **30** (1990) 277

36 P. W Terry, et al, *Advances in reversed field pinch theory and computation*, Plasma Phys. and Controlled Nuclear Fusion Res. (Proc. 13th Int. Conf., Washington, D.C., 1990), IAEA, Vienna (1991) 757

37 D.D. Schnack, *Magnetohydrodynamic theory of the reversed-field pinch dynamo*, in Physics of Alternative Magnetic Confinement Schemes, S. Ortolani and E.Sindoni, Eds., SIF, Bologna (1991) 631

D.D. Schnack et al., *Advances in reversed field pinch theory and computation*, Plasma Phys. and Controlled Nuclear Fusion Res. (Proc. 14th Int. Conf., Wuerzburg, 1992), IAEA, Vienna (1993)

38 Y.L. Ho, Nucl. Fusion **31** (1991) 341

39 C. Sovinec, University of Wisconsin-Madison, private communication 1992

40 H.P. Furth, J. Killeen, M.N. Rosenbluth, Phys. Fluids **6** (1963) 459

41 J.A. Holmes, B.A. Carreras, T.C. Hender, H.R. Hicks, V.E. Lynch, An, Diamond, Phys. Fluids **28** (1985) 261

42 S. Assadi, K. Sidikman, S.C. Prager Phys. Rev. Lett **69** (1992) 281

43 Y.L. Ho and G.G. Craddock, Phys. Fluids B **3** (1991) 721

44 J.A. Holmes, B.A. Carrerras, P.H. Diamond, V.E. Lynch, Phys. Fluids **31** (1988) 1166

45 A.R. Jacobson and R.W. Moses, Phys. Rev. A **20** (1984) 3335

46 K. Kusano and T. Sato, Nucl. Fusion **26** (1986) 1051

47 K. Kusano and T. Sato, Nucl. Fusion **27** (1987) 821

48 R.A. Nebel, E.J. Caramana, D.D. Schnack, Phys. Fluids B 1 (1989),1671

49 K. Kusano and T. Sato, Nucl. Fusion **30** (1990) 2075

50 E.J. Nilles, Y.L. Ho, S.C. Prager, D.D. Schnack, Bull. APS Div. Plasma Phys. **34**(9) (1989) 8P22, p.2147

51 J.A. Beckstead, PhD Thesis, University of Wisconsin-Madison, DOE/ER/53198-167

52 R.G. Watt and R.A. Nebel, Phys.Fluids **26** (1983) 1163

53 G.A. Chartas, PhD Thesis, University of Wisconsin-Madison DOE/ER/53198-181

54 E.E. Scime, PhD Thesis, University of Wisconsin-Madison DOE/ER/53198-194

55 A.E. Adler, R.M. Kulsrud, R.B. White, Phys. Fluids **23** (1980) 1375

56 R.B. White, in Handbook of Plasma Physics, Vol.1, edited by A.A. Galeev and R.N. Sudan (North-Holland, New York, 1983) 622

57 B. Coppi, J.M. Greene, J.L. Johnson, Nuclear Fusion **6** (1966) 101

58 H.Y.W. Tsui, Nucl. Fusion **28** (1988) 1543

59 Reportedly, one who contributed to an earlier version of the DEBS code gave it her own first name. Unfortunately, her last name has not accompanied this anecdote, so proper credit is not given.

60 C.M. Bishop, *An Intelligent Shell for the Toroidal Pinch,* Culham Laboratory report CLM-P845 (1988)

61 C.L.Platt, S.H. Robertson, IEEE Transactions on Plasma Science **19** (1991) 954

62 E.J. Zita, S.C. Prager, Y.L.Ho, D.D. Schnack, Bull. Intl. Sherwood Fusion Theory Conf., Santa Fe, NM (Apr.1992) 2C45

CHAPTER 2

COMPUTATIONAL MODEL

All calculations presented in this paper were generated with a 3D magnetohydrodynamic (MHD) code[1] with nonideal boundary conditions.[2,3] This program (DEBS) solves the pressureless, resistive, compressible MHD equations (in normalized Gaussian units), namely, Maxwell's equations and Ohm's Law:

$$\mathbf{B} = \nabla \times \mathbf{A} \qquad \mathbf{J} = \nabla \times \mathbf{B}$$

$$d\mathbf{B}/dt = -\nabla \times \mathbf{E} \qquad \mathbf{E} = \eta \mathbf{J} - \mathbf{v} \times \mathbf{B}$$

together with conservation of mass and conservation of momentum:

$$\frac{\partial \rho}{\partial t} = -\mathbf{v} \cdot \nabla \rho - \rho \nabla \cdot \mathbf{v} \qquad \rho \frac{\partial \mathbf{v}}{\partial t} = -\nabla P + \mathbf{J} \times \mathbf{B}$$

These can be reduced to the form:

$$d\mathbf{A}/dt = -\eta \mathbf{J} + \mathbf{S}\, \mathbf{v} \times \mathbf{b}$$

$$\rho d\mathbf{v}/dt = -\mathbf{S}\rho\, \mathbf{v} \cdot \nabla \mathbf{v} + \nu \nabla^2 \mathbf{v} + \mathbf{S}\, \mathbf{J} \times \mathbf{B}$$

where the Lundquist number $S = \tau_R/\tau_A = \frac{aB_0}{\eta}\sqrt{\frac{\mu_0}{\rho_0}}$, and the Alfvén time $\tau_A = a/v_A$. Times are normalized to the resistive diffusion time $\tau_R = \mu_0 a^2/\eta$,

velocities are normalized to the Alfvén velocity $v_A = B_0/(\mu_0\rho_0)^{1/2}$, and lengths are normalized to the plasma minor radius, a. The magnetic field B and mass density ρ are measured in units of a characteristic field B_0 and a characteristic density ρ_0, respectively. The viscous damping parameter ν is chosen for numerical stability; typical values of scalar ν are close to physically expected collisional values.[4] The gauge in which $\nabla\Phi=0$ has been chosen, where Φ is the electrostatic potential.

The DEBS code solves an initial value problem in **B**, **v**, **J**, and **A**, starting with modified Bessel-function model profiles typically chosen to yield a pinch parameter $\Theta = 1.59$. Density ρ and resistivity η profiles are not advanced in time, and toroidal flux is held constant once steady state is reached. Θ remains as constant as the plasma current I_p, whose allowed rate of change can be varied. In this as in previous studies, I_p is held constant to one part in 10^{12}, which sometimes leads to large oscillations in the loop voltage. Values of V_L referenced in this work represent the average value about which oscillations occur.

In all cases presented here, S is 6000, at least an order of magnitude lower than experimental values. Since $S \propto 1/\eta$, our numerical RFPs have higher resistivity, which results in a narrower numerical mode spectrum and smaller external kink modes than observed experimentally. Pressure is not included in this version of DEBS, therefore pressure gradient-driven modes such as Rayleigh-Taylor instabilities are not considered. These are expected to be far smaller than current gradient-driven modes.[5] A vanishing pressure gradient is valid for low-beta plasmas; this limits

differentiation of diffusion and dynamo timescales[6], but does not prevent accurate modeling of changes in profiles and flux surface reconnections characteristic of dynamo "sawteeth"[7]. When an evolving anisotropic pressure tensor is included in DEBS, profiles and flux surfaces evolve much as in DEBS with constant pressure, except that the sawtooth crash occurs on a much shorter timescale, as in experiments.[8]

Conducting wall boundary conditions are maintained as the MHD equations are advanced in time until a steady-state RFP equilibrium is reached. Signatures of steady state include saturated fluctuations (constant time-averaged amplitudes), spatially constant $E_z(r)$, and null $E_\theta(r)$, in agreement with $d\mathbf{B}/dt=0$. Resistive-shell boundary conditions are then imposed on this equilibrium, which is advanced with or without feedback. Resistive-shell RFPs typically evolve away from the initial equilibrium as fluctuations grow; these fail to reach a steady state. Feedback can nearly saturate fluctuations and restore $dB/dt=0$, bringing the RFP to a quasi-steady state.

DEBS pseudo-spectrally models a periodic cylinder of length $L=2\pi R$, where R is the major radius of a torus. Equations are finite-differenced radially and Fourier analyzed in the θ and z directions, following Nebel's corollary to Occam's Razor, "do everything where it's simplest"[9]. Linear terms are advanced in Fourier space, where derivatives can be expressed in terms of products with frequencies or mode numbers. Nonlinear terms are multiplied in configuration space, then de-aliased by truncating the top third of the spectrum[10]. Fast Fourier Transform (FFT) routines[11] are used

to translate terms back and forth between configuration and Fourier space as needed. Use of a semi-implicit algorithm eliminates Courant-Friedrichs-Lewy (CFL) time-step constraints due to Alfvén waves and allows tracking of phenomena on resistive diffusion timescales[12].

As few modes as necessary to model the RFP physics are included in a given run to keep costs in Cray time as low as possible. It has been shown numerically that m=2 modes dissipate energy cascaded to short wavelengths, thus are important in determining the width in n-space of the magnetic energy spectrum, but that $m > 2$ contribute little to RFP dynamics[13]. It has also been shown analytically[14] and experimentally[15,16] that the dominant helical modes have m=1, $n \approx -2R/a$, which resonate near the RFP axis. Higher-n modes (eg $-n \approx 4R/a$) resonate closer to the plasma edge, are spaced more closely together, and have amplitudes an order of magnitude lower, at least at S=6000. Modes couple as $(m,n) + (m',n') \rightarrow (m \pm m', n \pm n')$. Therefore, the smallest scale m=2 modes of significance will have $-n \approx 8(R/a)$. Therefore, to include all modes important in the present study, $m=0,\pm1,\pm2$ and $n=0,\pm1,\pm2,\ldots,\pm(8R/a)$ are retained after de-aliasing. The radial grid must be fine enough to resolve the smallest-wavelength modes present. For the R/a=2.5 and R/a=6.0 cases presented here, we choose $\Delta r=a/127$. In lower-aspect ratio cases, resonant modes have longer wavelengths, therefore $\Delta r=a/63$ can give adequate profile resolution. While lower-aspect ratio runs advance faster, they exacerbate the underestimation of nonlinear interactions already imposed by the artificially high resistivity of low-S cases.

References

1 D.D. Schnack, D.C. Barnes, Z. Mikic, D.S. Harned, E.J. Caramana, Jrnl. Comput.Phys. **70** (1987) 30

2 Y.L. Ho, S.C. Prager, Phys. Fluids **31** (1988) 1673

3 E.J. Nilles, S.C. Prager, Y.L.Ho, Bull. Am. Phys. Soc. **34** (1989) 2147

4 Y.L. Ho and S.C.Prager, Phys. Fluids B **3** (1991) 3099

5 S. Cappello and R. Paccagnella, Phys. Fluids B **4** (1992) 611

6 C.G. Gimblett and D.D. Schnack, *Simulation of the thin shell and secondary shell HBTX1C experiments,* Science Applications International Corporation SAIC-91/1016:APPAT-140 (1991)

7 D.D. Schnack, *Magnetohydrodynamic theory of the reversed-field pinch dynamo,* in Physics of Alternative Magnetic Confinement Schemes, S. Ortolani and E.Sindoni, Eds., SIF, Bologna (1991) 631

8 D.D. Schnack et al., *Advances in reversed field pinch theory and computation,* Plasma Phys. and Controlled Nuclear Fusion Res. (Proc. 14th Int. Conf., Wuerzburg, 1992), IAEA, Vienna (1993)

9 Rick Nebel, via Ken Sidikman, private communication

10 D.D. Schnack, D.C. Baxter, E.J. Caramana, J Comp Phys. **55** (1984) 1485

11 D. Gottleib, S.A. Orszag, Numerical Analysis of Spectral Methods (SIAM, Philadelphia, PA 1977)

12 C.G. Gimblett and D.D. Schnack, *Simulation of the thin shell and secondary shell HBTX1C experiments,* Science Applications International Corporation SAIC-91/1016:APPAT-140 (1991)

13 J.A. Holmes, B.A. Carrerras, P.H. Diamond, V.E. Lynch, Phys. Fluids **31** (1988) 1166

14 J.B. Taylor, Rev. Mod. Phys. **58** (1986) 741

15 R.J. LaHaye, P.S.C. Lee, M.J. Schaffer, T. Tamano, P.L. Taylor, Nucl.Fusion **28** (1988) 918

16 A. Almagri, S. Assadi, J. Beckstead, et al., *Edge Fluctuations in the MST Reversed Field Pinch,* in Physics of Alternative Magnetic Confinement Schemes, S. Ortolani and E. Sindoni, Eds., Societa Italiana di Fisica, (1991) 223

CHAPTER 3

$B_r(m,n)|_a=0$ FEEDBACK WITH CONDUCTING HELICAL COILS

3.0 Introduction

Our numerical experiment comprises a number of nonlinear resistive-shell RFP runs which suppress several subsets of tearing modes with the feedback scheme described below. We seek to characterize the smallest subset of feedback-targeted modes for which plasma parameters approach the conducting-shell case. Effective feedback should minimize mode growth and loop voltage in the absence of a conducting shell, while maintaining the reversed-field configuration.

The most effective feedback schemes target the subset of candidate dynamo modes which provides the greatest contribution to both the RFP dynamo (via the fluctuation-induced electric field E_F) and loop voltage V_L. Feedback decreases the amplitude of targeted modes below their resistive-shell levels and causes a shift of magnetic energy into m=1 modes with nearby resonant surfaces r_s (defined where $q(r_s)=m/n$), therefore also nearby in mode-number-space. As dominant modes are stabilized, they lose their dynamo character. As neighboring modes grow, they assume dynamo form. These newly-dominant fluctuations provide

the RFP dynamo, sustaining reversal in the absence of a conducting shell. The fluctuation-driven parallel electric fields of the new dynamo modes approach conducting-shell E_F profiles, sustaining reversal with low loop voltage, which may reduce transport.

In this chapter, we describe the physical representation and our numerical implementation of one feedback scheme (3.1). We test this scheme on a range of modes individually (3.2), then simultaneously in various combinations (3.3). We present results for small aspect-ratio (skinny) RFPs (3.3.a) and large aspect-ratio (fat) RFPs (3.3.b), and we compare our numerical results with experimental tests (3.3.c)

3.1 Feedback scheme: conducting helical coils

Feedback boundary conditions are applied numerically to a mode (m,n) targeted for stabilization by specifying that $B_r(m,n)$ vanish at r=a, where a resistive shell provides a physical boundary at the plasma edge. The pseudospectral nature of DEBS is exploited to impose boundary conditions on each helical mode independently. In Fourier space, $B_r=(\nabla\times A)_r=i(mA_z/r-kA_\theta)$, assuming quantities vary as $f(r)e^{i(m\theta + kz + \phi)}$ where $k=n/R$ is the axial wavenumber. Choosing $B_r=0$ determines $A_\theta(m,n)$ and $A_z(m,n)$ for the targeted mode at r=a, consistent with the remaining boundary conditions: that $J_r=0$, $E_\theta(a)=0$, $E_z(a)=$ the applied edge field necessary to sustain plasma current density $J_{||}$, and $v(a)=0$ for all modes except $v_r(a)=-E_zB_\theta/SB^2$ for the mean.[1]

The feedback boundary conditions can be realized experimentally by winding helical current-carrying coils on the resistive shell. The feedback scheme is equivalent to a set of helical coils (one sine and one cosine) to stabilize each mode (m,n), wound with the same pitch as the magnetic field line at r_s with which the mode resonates. The helical coils are perfectly conducting, drawing whatever current necessary to keep $B_r(m,n)|_{a=0}$ for the targeted mode. There is no time delay between "sensing" an edge B_r and nulling it, and the feedback response is perfectly out of phase with the target mode.

Only harmonics of the targeted mode are directly stabilized by feedback. For example, application of $B_r|_{a=0}$ feedback to (m,n) = (1,-5) also stabilizes the (2,-10) mode. Since modes with m>1 serve primarily as an energy dissipation channel, damping them should tend to destabilize the RFP by partially blocking the m=2 energy sink. Indirect stabilization of neighboring tearing modes via quasilinear coupling of feedback through (m=0,n≠0) modes also yields destabilization, in general. Therefore, any stabilization of nonharmonic modes arises from nonlinear interactions with modes to which feedback is applied directly.

3.2 Single-mode feedback

We performed nonlinear calculations for an aspect ratio R/a=2.5 RFP with S=6000 and θ=1.59. When the conducting shell at r=a is replaced with a resistive shell, loop voltage rises (Figure 3.1) and reversal is lost on

the order of a shell time (Figure 3.2). Loop voltage grows faster than the shell timescale ($\tau=.68\tau_s$ if $V_{no} = V_c\, e^{t/\tau}$, where V_{no} is the loop voltage in a resistive shell without feedback and V_c is the loop voltage in a conducting shell) in an effort to sustain the plasma current. (This is probably a pessimistic estimate, since current is held more constant than typical in experiments, in order to make V_L comparisons between runs.) Numerical tests were performed for two cases to test the feasibility of edge feedback on one internal tearing mode. $B_r(a)=0$ was imposed on the (m=1,n=-5) mode in one case and on the (1,-7) mode in another case. These were originally the dominant dynamo modes, typically resonating around r=.4a and r=.6a, respectively. Feedback on either dynamo mode sustains reversal and lowers loop voltage for at least three shell times beyond the time shown in Fig.3.1. Steady-state parameters for various feedback cases are compared in section 3.3.a below.

Without feedback (Fig.3.3.a), E_F at the edge is insufficiently negative to sustain reversal. Correspondingly, V_L quadruples in a shell time. With (1,-5) feedback, not only is reversal sustained, but loop voltage is restored to within 30% of the conducting shell level as E_F drops throughout the plasma (Fig.3.3.b). Feedback control of (1,-7) is not as effective in reducing V_L, pointing to a significant sensitivity to choice of target mode. Based on these single-mode feedback results, we attempt to more closely approach the conducting shell case by applying feedback to several modes simultaneously.

3.3 Multi-mode feedback

3.3.a Small aspect ratio: R/a=2.5

With either a conducting or resistive shell, tearing modes with m=1 and $|n|$≈4-8 dominate energy spectra in an RFP with aspect ratio R/a=2.5. The dominant m=1 modes tend to be separated by Δn=2, as the (0,2) mode is the largest axially symmetric fluctuation. Depending on the random amplitudes of initialized perturbations, we have found quasi-steady states where either (1,-5) and (1,-7) or (1,-4) and (1,-6) dominate the mode spectrum on the order of a shell time. (Global plasma parameters such as mean field levels and profiles are generally independent of initalization.) These internally resonant helical fluctuations grow on the order of the resistive shell time in the absence of feedback. Loop voltage grows on a faster timescale in order to hold the plasma current constant. Most of the results presented here are from the conducting shell steady state dominated by (1,-5) and (1,-7) fluctuations; results are comparable for the initialization dominated by (1,-4) and (1,-6) fluctuations.

Since the few m=1 modes with $|n|$ between 2R/a and 3R/a typically account for almost 90% of the fluctuation magnetic energy, we ran numerical tests of feedback on different combinations of these modes. Multi-mode feedback is applied to two and four modes in several combinations.

Feedback is applied to two modes simultaneously in four different cases: to (1,-5) and (1,-7); to (1,-4) and (1,-6); to (1,-5) and (1,-6). In a fourth

test, feedback is applied to (1,-5) and (1,-7) until (1,-4) and (1,-6) become dominant, after which time feedback is applied to (1,-4) and (1,-6). The (1,-5) tends to provide the bulk of the dynamo E_F in the absence of feedback. Stabilization of (1,-5) is common to the most effective feedback schemes: this channels energy into the (1,-4) and (1,-6) modes, which sustain dynamo with lower E_F. Feedback on (1,-4) or (1,-6), on the other hand, forces more energy into the original dynamo modes, (1,-5) and (1,-7), increasing fluctuations and V_L.

We also apply feedback to all four candidate dynamo modes simultaneously (m=1, $|n|$=4-7). In this case, energy does not flow into modes outside the candidate dynamo range, but peaks in (1,-5) as before. Results are summarized in Fig. 3.4, which shows the approach of plasma loop voltage to the level in a conducting shell as feedback is applied to different modes. In all schemes which target (1,-5), growth rates approach zero for all modes as the feedback-stabilized RFP approaches steady state.

Improvement in plasma parameters of resistive-shell RFPs with feedback is due not simply to reductions in fluctuation levels, but to changes in E_F profiles. While feedback on (1,-5) reduces the magnetic fluctuation energy

$$W_m = \frac{1}{2}\int_{volume} b^2(m,n)\,d\tau$$

and the velocity fluctuations or kinetic energy

$$W_k = \frac{1}{2}\int_{volume} v^2(m,n)\,d\tau$$

in the targeted mode, energies rise correspondingly in neighboring modes such as the (1,-7) and (1,-6). Similarly, (1,-7) feedback reduces W_m and W_k in (1,-7) while (1,-5) and (1,-6) fluctuations rise. However, changes in W_m and W_k summed over all modes correlate only roughly with changes in V_L. (Figures 3.4-3.6). There are cases (for example, with (1,+2) feedback) in which the overall fluctuation levels increase with feedback, yet the relative phasing and spatial distribution of individual fluctuations change such that volume-averaged E_F decreases, lowering V_L and sustaining reversal.

Decomposition of $(E_F)_\theta = -S\langle \mathbf{v}\times\mathbf{b}\rangle_\theta = v_r b_z - v_z b_r$ for many feedback cases shows that in resistive-shell RFPs the $v_r b_z$ term drives most of the negative mean E_θ, or dynamo, at the plasma edge in resistive-shell RFPs (Fig.3.7a). This is consistent with predictions for compressible plasmas.[2] In conducting-shell RFPs, it is $v_z b_r$ which accounts for dynamo drive, since v_r is very small throughout the reversal region. (Earlier incompressible numerical simulations with $v_r \equiv 0$ found[3] no RFP dynamo; our results emphasize the importance not of nonzero $v_r(a)$ but of incompressibility ($\nabla \cdot v = 0$) for the RFP dynamo.) Examination of $(E_F)_Z = v_\theta b_r - v_r b_\theta$ reveals that both terms contribute nearly equally to loop voltage (Fig.3.7b) in all cases. Experimental measurement of these terms is planned.[4]

3.3.b Details of three R/a=2.5 cases

In the remainder of this section, we examine a limited set of runs in more detail to discern the mechanisms responsible for effective feedback. We focus on the simultaneous feedback of (1,-5) and (1,-7) modes in a resistive shell, and compare this case to the resistive shell without feedback (worst case) and to the conducting shell (best case), which effectively applies feedback to all fluctuations.

Fig.3.8 shows magnetic energy spectra for the three cases after evolution for one shell time. In the conducting-shell case (Fig.3.8.c), (1,-5) and (1,-7) are the dominant fluctuations. With a resistive shell (Fig.3.8.a), all modal energies grow approximately an order of magnitude in one shell time; that is, mode amplitudes triple. The (1,-5) mode remains dominant and (1,-6) has grown nearly as large as (1,-7). When feedback is applied to the two dominant modes simultaneously (Fig 3.8.b), the (1,-5) and (1,-7) amplitudes drop below conducting-shell levels. All other modes grow beyond conducting-shell levels, and the neighboring modes (1,-4) and (1,-6) become dominant. Reversal is maintained past three shell times, when we choose to terminate the run. (Large velocity fluctuations in the case without feedback make the time step size too small to justify continuing our tests beyond this point.)

Changes in modal $E_F(m,n)$ profiles follow the same pattern for all cases when feedback is applied to the dominant modes: these lose their dynamo character and the newly-dominant m=1 modes spontaneously

alter to provide the dynamo instead. In the conducting-shell case, (1,-5) and (1,-7) drive dynamo with negative E_F in the reversal region. When feedback is applied to these modes they lose their dynamo character, contributing negligible E_F in the reversal region (Fig.3.9). The (1,-6) and (1,-4) were small and non-dynamo with a conducting shell. But with feedback these neighboring modes adjust to provide negative E_F in the reversal region (Fig.3.10, curve b), taking on the dynamo role. (This process is representative of all feedback cases examined. For example, in the initialization which yields dominant (1,-4) and (1,-6) in steady state, feedback on these modes causes them to lose their dynamo character, while neighboring (1,-5) and (1,-7) grow to provide the dynamo.) As in single-mode feedback, reduced E_F keeps $E_{||}$ and V_L low for a given plasma current.

Data suggest that feedback stabilization also reduces magnetic field line stochasticity, thereby reducing transport[5] of particles and energy to the plasma edge. In a perfectly conducting shell, most flux surfaces near the plasma edge are closed, forming m=0 magnetic islands around the reversal surface r_V. Without feedback, $B_r(a)\neq 0$ and many flux surfaces near the edge intersect the wall, carrying with them particles and energy. Figure 3.11 plots helical flux[6] through contours of constant z through a circle of radius r, for m=0 modes. These all resonate at the reversal surface, where B_Z vanishes. When feedback is applied to the dominant tearing modes, fewer flux surfaces reach to the wall, as seen in Fig.3.11. This is partly due to decreased driving of the edge modes (m=0; m=1, n≥10) by current

gradients and partly due to a radially inward shift of the m=0 islands. The current parallel to the magnetic field, $\mu = \frac{\mathbf{J}\cdot\mathbf{B}}{B^2}$, exhibits small gradients near the plasma edge in both the conducting shell and the feedback case, while the edge gradient steepens markedly in the resistive shell case without feedback (Fig.3.12). Decreased μ around $r=r_V$ shrinks m=0 islands and reduces plasma-wall interaction.

While feedback restores confinement in the plasma edge region, it also pushes internal modes toward the plasma axis. This is evident for the m=0 modes above. For m=1 modes, we examine helical flux contours which map the amount of flux through a ribbon[6] stretched between the magnetic axis and a helix with $m\theta + nkz$ = constant. Like values of flux are connected across the point of maximum flux, at the resonant surface where $q(r_S)=-m/n$. A helical flux plot over a poloidal cross section yield an image of the (m,n) magnetic islands. Fig.3.13 illustrates that tearing modes move outward in radius with a resistive shell and inwards with feedback. This is verified by calculating resonant surfaces for the modes. Not only the targeted modes but also neighboring tearing modes are moved radially inward by feedback, even when their magnetic fluctuations grow. This is consistent with observed changes in profiles of the safety factor q, which determines the location of resonant surfaces. Feedback decreases q in the region of the dominant modes, as seen in Fig.3.14; this moves resonant surfaces inward, compared to the resistive shell case.

A scenario for the mechanism of feedback stabilization emerges from our investigations. When $B_r(m,n)|_a = 0$ is applied to a dominant m=1 tearing mode resonant near axis, the mode's global B(r) and v(r) amplitudes decrease. As E_F drops on axis, J near axis can grow. This decreases the safety factor near resonant surfaces of dominant modes, shifting r_s inward for axially resonant modes. Deeper resonant surfaces result in relatively larger dynamo-driving regions of negative $(E_F)_\theta$ outside each $r_s(m,n)$. The net effect, as demonstrated above, is more RFP dynamo and less loop voltage.

The axial and helical flux plots in Fig.3.11 and Fig.3.13 do not give a complete picture of field line stochasticity. Poincare or puncture plots would more precisely track transport along field lines. While Poincare plots are not yet available for the data shown, it has been observed in previous works that flux plots and Poincare plots similarly track field line intersections with the wall, while Poincare plots illustrate stochasticity in the RFP core.

3.3.c Large aspect ratio: R/a=6.0

The number of dominant modes is about 2R/a. Hence, feedback can be more difficult at large aspect-ratio. In the limit of low beta[7], the safety factor on axis approaches $q=aB_Z(0)/RB_\theta(a)$. Since $B_Z \approx B_\theta$, the safety factor on axis decreases as R/a increases, as seen in Fig.3.15. Therefore the dominant fluctuations have higher n-number and are more closely spaced

than in the small aspect-ratio cases considered above, Tearing modes are more strongly coupled to each other; mode amplitudes and growth rates are also greater at large aspect ratio. In the absence of feedback, magnetic energy fluctuations grow and the loop voltage increases a factor of four in one shell time, as seen in Fig.3.16.

All internal m=1 modes in the range (1,-11) to (1,-18) contribute readily to the dynamo when R/a=6.0. If feedback is applied to any one of these candidate dynamo modes, energy in that mode simply shifts into near neighbors. However, unlike the small-aspect ratio case, such a shift in the energy spectrum does not tend to lower the loop voltage. Feedback on (1,-13) alone, which tends to be slightly larger than the other dynamo modes, is insufficient to improve the efficiency of neighboring dynamo modes. Several m=1 modes must be stabilized simultaneously; significant loop voltage reduction is evident when the number of modes stabilized approaches the aspect ratio (case v in Fig.3.16).

As an auxilliary method, we investigate feedback not just on m=1, but also on modes which play a role in m=1 coupling. Since m=1 modes couple to each other quasilinearly through m=0 modes as well as nonlinearly, m=0 feedback is added. If feedback of m=0 modes also reduced amplitudes of m=1 modes to which they couple, then feedback on only a few m=1 modes may suffice with simultaneous feedback on m=0. Combining m=1 feedback with (0,2) feedback is observed to reduce plasma V_L and feedback coil currents only to a moderate extent. Feedback on a wide range of candidate dynamo modes more closely approaches the conducting shell

case.

Currents required by feedback coils (J_{FB}) remain relatively low, regardless of aspect ratio. Feedback coil currents are calculated from the discontinuity of the tangential component of the magnetic field at the surface r=a between the plasma edge and the coil. Since the magnetic field vanishes inside a perfectly conducting coil, the jump condition[8]

$$\mathbf{n}\times(\mathbf{H_2}-\mathbf{H_1})=\frac{4\pi}{c}\mathbf{K}$$

becomes

$$\frac{1}{\mu}\left(0-\mathbf{B}_{plasma}(a)\right)\propto\frac{4\pi}{c}\mathbf{J}_{coil\perp}$$

or

$$\mathbf{B}_\theta(a)\propto\mathbf{J}_z \qquad \text{and} \qquad \mathbf{B}_z(a)\propto\mathbf{J}_\theta$$

Feedback coil currents are normalized to currents driving the mean plasma field:

$$\frac{J_{coil}(m,n)}{J(0,0)}=\frac{\sqrt{B_{z,coil}{}^2(m,n)+B_{\theta,coil}{}^2(m,n)}}{\sqrt{B_z{}^2(0,0)+B_\theta{}^2(0,0)}}$$

At most, a total of $\Sigma J_{coil}/J_{(0,0)} \equiv 8.5\%$ is required when five dynamo modes are simultaneously stabilized. This decreases loop voltage by 60%, for a net reduction in input power requirements. These results suggest that if space constraints are not severe, coils resonant with m=1, $2R/a < n < 3R/a$ should be wound for possible use in feedback stabilization in RFP experiments. Addition of a (0,2) winding may provide additional feedback system flexibility.

3.4 Comparison with experiment

3.4.a Feedback on HBTX

The HBTX1C RFP (R/a=3.0) experiment[9] experienced higher fluctuation levels and truncated plasma discharge times when its conducting wall was replaced with a resistive shell. Reversal loss was attributed to growing resistive shell modes. The resistive internal (1,-5) and ideal external (1,2) modes were observed to grow at similar rates at θ=1.6, contrary to predictions of linear theory,[10] suggesting close nonlinear coupling between the modes. The internal mode resonates near the plasma axis, but the external mode is nonresonant. This suggested that feedback coils at the wall (r=1.1a) might more effectively suppress the free boundary (1,2) mode. It was hoped that suppression of (1,2) would couple to suppress (1,- 5) also, thereby sustaining the RFP. Feedback coils were wound outside a secondary shell at 1.1a with a 5.5 ms vertical field soak-in time. Reversal persisted up to two shell times with application of (1,2) feedback, but loop voltage and fluctuation levels remained high.[11]

3.4.b MHD computations

Our low-aspect ratio calculations[12] model an RFP similar in size to HBTX . It should be noted that the high resistivity (low S) in our calculations, relative to experiment, yields smaller external kinks, such as the (1,2) mode.[13]

We modeled an idealization of the experimental feedback (which reduced B_r at r=1.1a with a finite time lag) with calculations that nulled B_r at r=a at all times. Our computations show that edge feedback on the (1,2) mode, resonant near the plasma edge, is less effective than edge feedback on a tearing mode resonant near axis. As seen in Fig.3.2, the resistive shell RFP loses reversal on the order of a shell time. Feedback on the external (1,2) mode makes edge E_F sufficiently negative to sustain reversal (Fig.3.17), but fluctuation levels and V_L remain high, as in HBTX1C. While reversal lost with a resistive shell is restored with feedback on either the (1,2) or (1,-5) mode, only the latter also reduces V_L (Fig.3.4). This is because axial E_F remains high with (1,2) feedback (Fig.3.17a), while (1,-5) feedback leads to reduced E_F throughout the plasma (Fig.3.3.b).

The similarity of experimental and numerical results suggests that even ideal feedback applied to external modes such as (1,2) is of limited use on an RFP. It is more effective to target the m=1 dynamo modes directly, instead of relying on coupling with externally resonant modes targeted for feedback. This is consistent with observations that axially resonant m=1 tearing modes drive RFP dynamics, through quasilinear modifications of mean field profiles and through nonlinear interactions with each other[14,15]. That edge feedback has a strong effect on dynamo modes even though they are resonant deep within the plasma need not be surprising in light of calculations[16] which found internal m=1 modes' dependence on boundary conditions to be highly nonlinear.

3.5 Physical mechanism for effective feedback

Since central E_F drops, the newly-dominant m=1 modes sustain the RFP more efficiently than the original, feedback-stabilized dynamo modes. The efficiency of the new dynamo modes can be quantified in terms of the ratio of dynamo-driving poloidal E_F near the RFP edge to current-suppressing toroidal E_F near the core. We define $\varepsilon = \langle E_{F\theta} \rangle_{edge} / \langle E_{Fz} \rangle_{core}$, where $\langle\ \rangle_{edge}$ is a volume average from r_m to r=a and $\langle E_{Fz} \rangle_{core}$ is a volume average from r=0 to r_m, where the poloidal and toroidal fields have the same magnitude at r_m. For example, the (1,-6) dynamo mode in the feedback case yields $\varepsilon \cong 21\%$. Without feedback the same dynamo mode has only $\varepsilon \cong 11\%$ (Fig.3.3), and significantly higher V_L is required to maintain the plasma current.

A scenario for the mechanism of feedback stabilization emerges from our investigations. When $B_r(m,n)|_a = 0$ is applied to a dominant m=1 tearing mode resonant near the axis, the mode's global B(r) and v(r) amplitudes decrease. As E_F drops on axis, central J can grow. This decreases the axial safety factor, shifting r_s inward for axially resonant modes. Deeper resonant surfaces result in relatively larger dynamo-driving regions of negative $(E_F)_\theta$ outside each $r_s(m,n)$. The net effect, as demonstrated above, is more RFP dynamo and less loop voltage.

3.6 Summary

A simple feedback scheme has been developed to stabilize resistive shell fluctuations without suppressing the RFP dynamo. Investigation by nonlinear MHD computations on RFPs of large and small aspect ratio reveal that feedback on a small number (~R/a) of m=1 modes restores RFP reversal and lowers loop voltage. Edge feedback on axially resonant m=1 dynamo modes proves more effective than edge feedback on

free-boundary modes resonant near the edge. A physical mechanism for feedback stabilization is proposed. Feedback tests also reveal optimal <vxb> profiles for dynamo efficiency and show that $v_r b_z$ provides the bulk of the resistive-shell RFP dynamo. Results agree with a limited experimental test of feedback on an external mode. Feedback stabilization of dominant internally resonant tearing modes is predicted to extend plasma discharge duration times and reduce required loop voltage. This has yet to be tested experimentally.

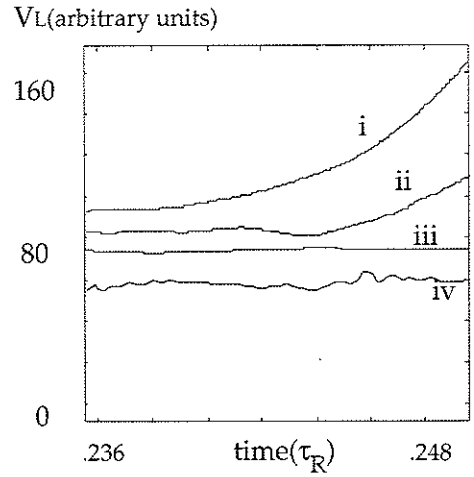

Figure 3.1: Loop voltage versus time for four R/a=2.5 cases:
(i) resistive shell without feedback
(ii) resistive shell with feedback on the (m=1, n=-7) mode
(iii) resistive shell with feedback on (1,-5) mode
(iv) close-fitting conducting shell.

(The (quasi-)steady state values reached by the loop voltage in each case at later times can be seen in Fig.3.4)

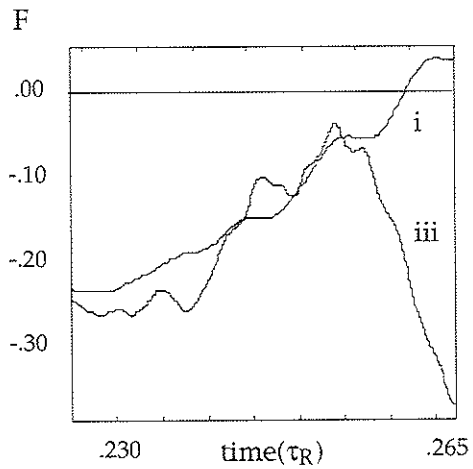

Figure 3.2: Reversal parameter F versus time for
(i)resistive shell without feedback
(iii) resistive shell with feedback on (1,-5) mode.

F fluctuates about a mean value of -.20 with feedback in quasi-steady state (evident at later times), never losing reversal.

Fig.3.3.a

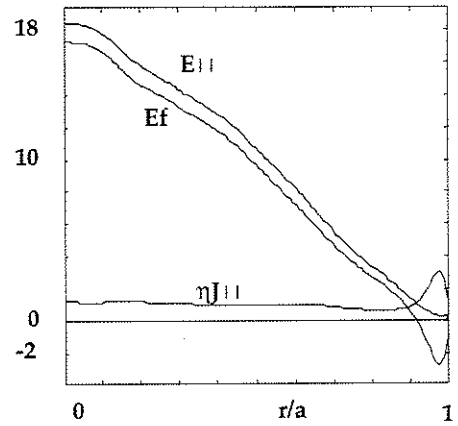

Fig.3.3.b

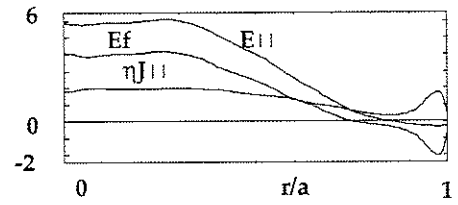

Fig.3.3 Radial profiles of total parallel electric field $E_{||}=E_f + \eta J_{||}$, E_f, and $\eta J_{||}$ where the parallel fluctuation-induced electric field $E_f = -S\langle vxb\rangle.B/|B|$:
(a) without feedback
(b) with (1,-5) feedback

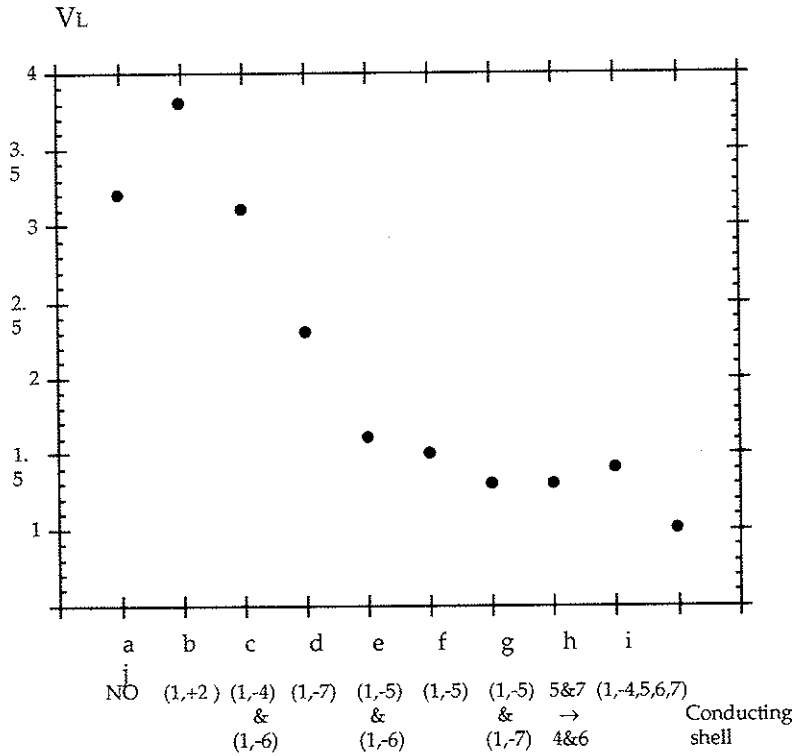

Fig.3.4: Loop voltage (normalized to VL in conducting shell case) versus feedback case, for R/a=2.5 RFP with resistive shell:
(a) no feedback
(b)-(i): feedback on following modes (m,n):
(b) (1,+2)
(c) (1,-4) and (1,-6)
(d) (1,-7)
(e) (1,-5) and (1,-6)
(f) (1,-5)
(g) (1,-5) and (1,-7)
(h) (1,-5) and (1,-7), then (1,-4) and (1,-6)
(i) (1,-4). (1,-5), (1,-6), (1,-7) simultaneously
(j) conducting shell (all modes stabilized)

Fig.3.5 Wm

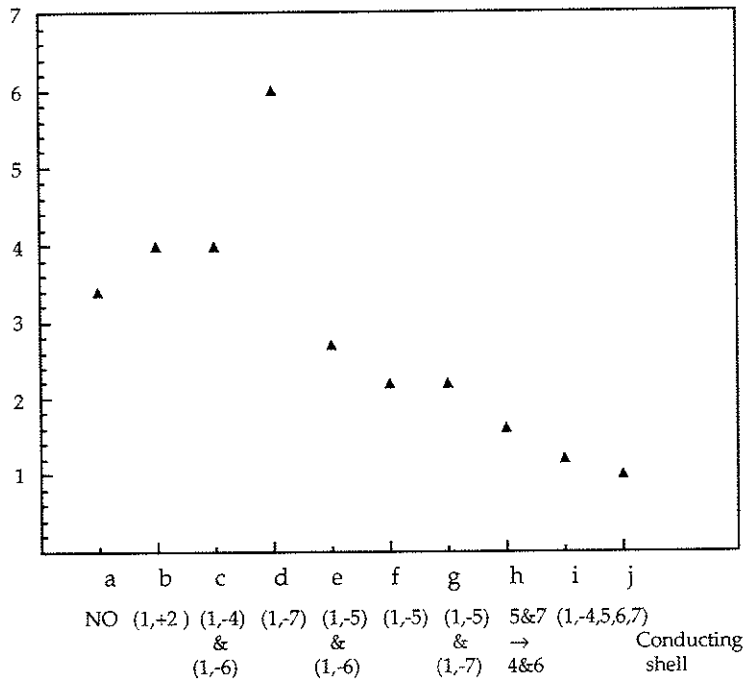

Fig.3.5: Magnetic energy summed over all fluctuations (normalized to conducting shell case) versus feedback case:
(a) no feedback
(b)-(i): feedback on following modes (m,n):
(b) (1,+2)
(c) (1,-4) and (1,-6)
(d) (1,-7)
(e) (1,-5) and (1,-6)
(f) (1,-5)
(g) (1,-5) and (1,-7)
(h) (1,-5) and (1,-7), then (1,-4) and (1,-6)
(i) (1,-4). (1,-5), (1,-6), (1,-7) simultaneously
(j) conducting shell (all modes stabilized)

Fig.3.6 Wk

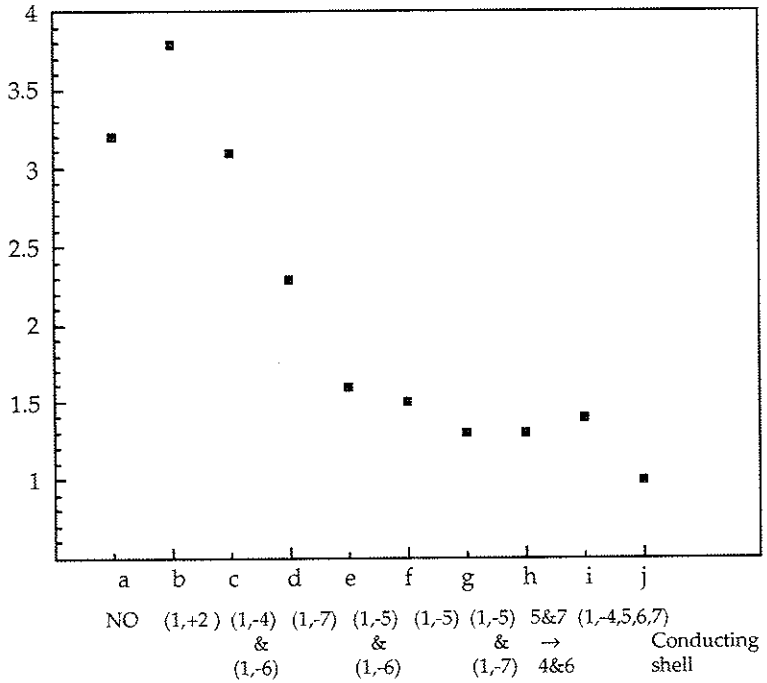

Fig.3.6: Kinetic energy summed over all fluctuations
(normalized to conducting shell case) versus feedback case:
(a) no feedback
(b)-(i): feedback on following modes (m,n):
(b) (1,+2)
(c) (1,-4) and (1,-6)
(d) (1,-7)
(e) (1,-5) and (1,-6)
(f) (1,-5)
(g) (1,-5) and (1,-7)
(h) (1,-5) and (1,-7), then (1,-4) and (1,-6)
(i) (1,-4). (1,-5), (1,-6), (1,-7) simultaneously
(j) conducting shell (all modes stabilized)

Fig.3.7.a

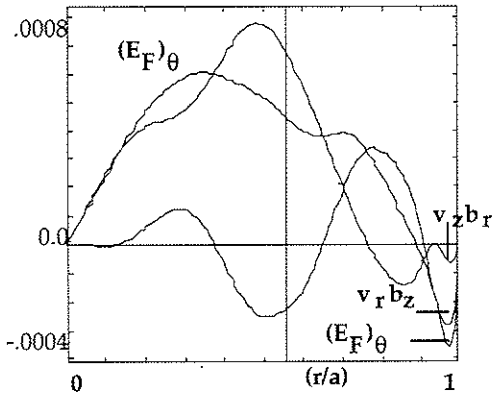

Fig.3.7.b

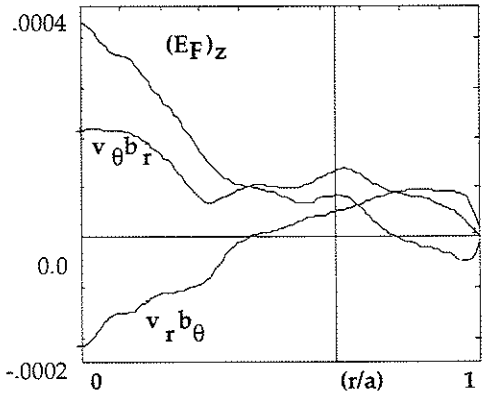

Fig.3.7: Resistive-shell profiles of:

(a) components of $(E_F)_\theta = v_r b_z - v_z b_r$ for (1,-5)

(b) components of $(E_F)_z = v_\theta b_r - v_r b_\theta$ for (1,-6)

Fig.3.8.a

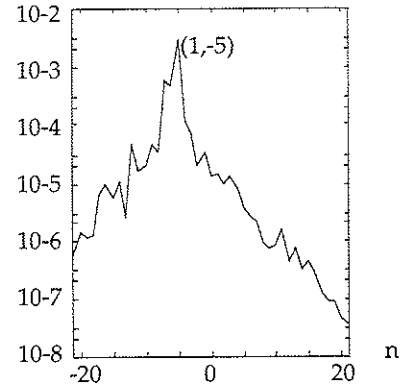

Fig.3.8.b

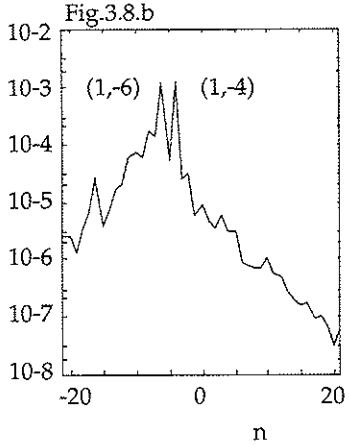

Fig.3.8.c

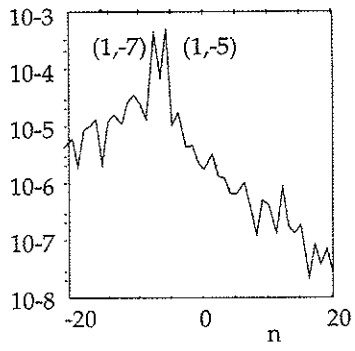

Fig.3.8: Spectra of m=1 magnetic energy fluctuations (volume-averaged) versus toroidal mode number n, after 1 shell time:
(a) resistive shell without feedback
(b) resistive shell with (1,-5) and (1,-7) feedback
(c) conducting shell

Fig.3.9

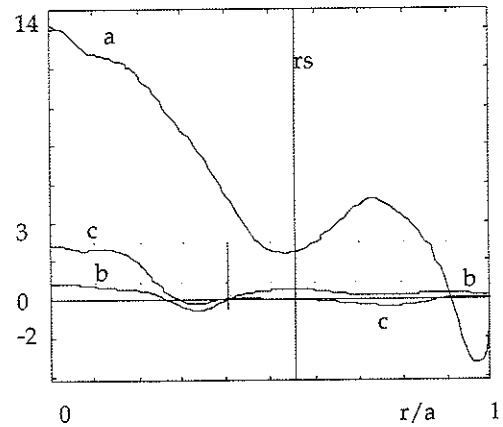

Fig.3.9: Profiles of modal (1,-5) fluctuation-induced electric field $E_F = -\langle v \times b \rangle \cdot B / |B|$ for
(a) resistive shell without feedback
(b) resistive shell with(1,-5)&(1,-7) feedback
(c) conducting shell.

Long vertical line is the resonant surface r_s without feedback; short vertical line is r_s for cases (b) and (c).

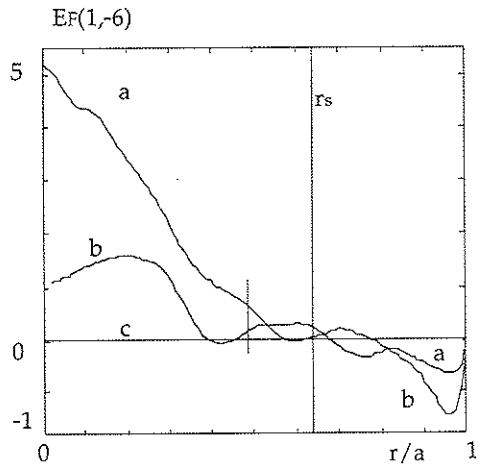

Fig.3.10: Profiles of modal (1,-6) fluctuation-induced electric field $E_F = -\langle v \times b \rangle \cdot B / |B|$ for:
(a) resistive shell without feedback
(b) (1,-5)&(1,-7) feedback
(c) conducting shell: E_F oscillates about zero at too low a level to distinguish, on this scale.

Long vertical line is the resonant surface r_s without feedback; short vertical line is r_s for cases (b) and (c).

Fig.3.11.a

Fig.3.11.b

Fig.3.11.c

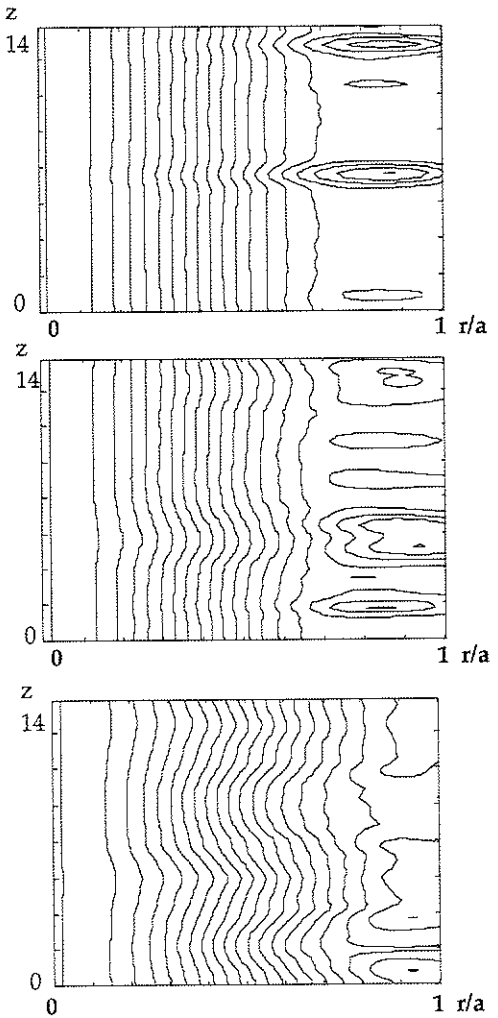

Fig.3.11: Flux contours (toroidal versus radial) for m=0
(a) conducting shell
(b) resistive shell with (1,-5) and (1,-7) feedback
(c) resistive shell without feedback

Fig.3.12.a

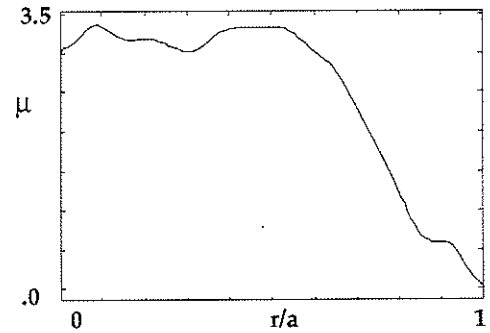

Fig.3.12.b

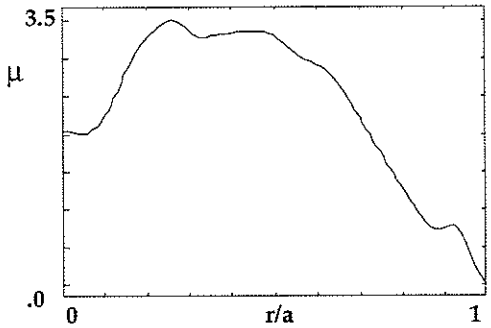

Fig.3.12.c

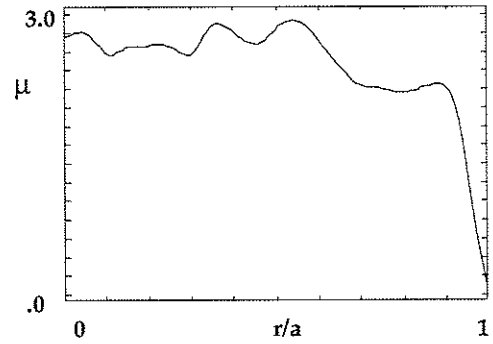

Fig.3.12: $\mu = \mathbf{J} \cdot \mathbf{B} / B^2$ versus radius for:
(a) conducting shell
(b) resistive shell with (1,-5) and (1,-7) feedback
(c) resistive shell without feedback

Fig.3.13.a

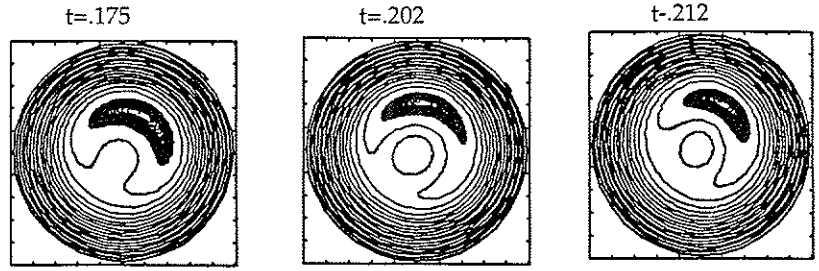

Fig.3.13.b

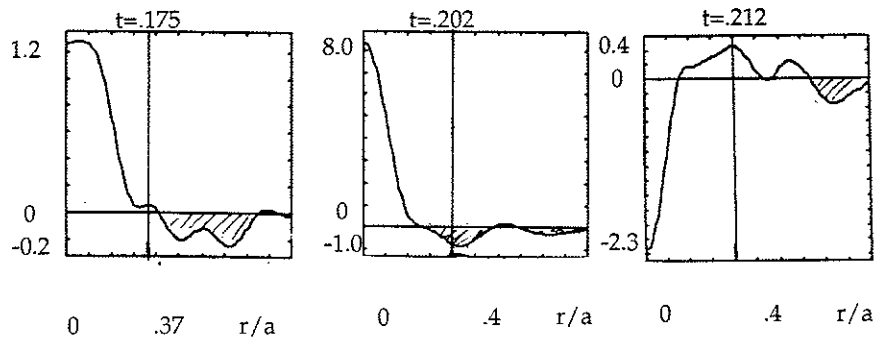

Fig.3.13: The (1,-5) island moves only slightly outward in a resistive shell with (1,-5)&(1,-7) feedback. (All times are normalized to the resistive diffusion time τ_R.)

(a) helical flux plots over a poloidal cross section
(b) Ef versus radius, with resonant surface indicated by vertical line

Fig.3.13.c

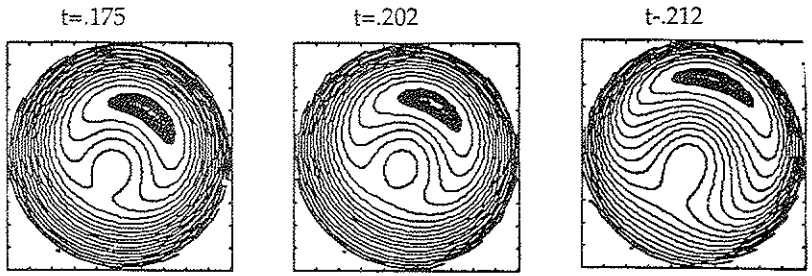

Fig.3.13.d

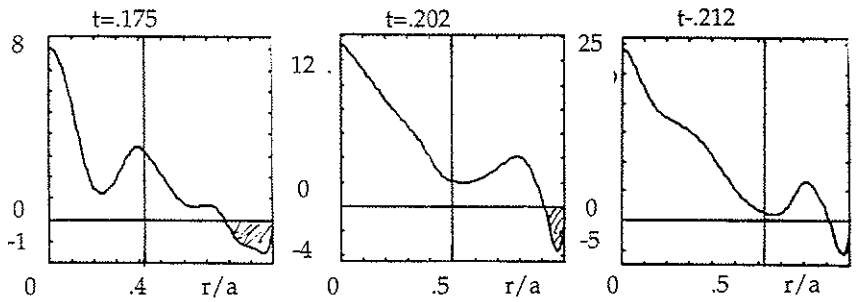

Fig.3.13: The (1,-5) island moves radially outward in a resistive shell without feedback. (All times are normalized to the resistive diffusion time τ_R.)

(c) helical flux plots over a poloidal cross section
(d) Ef versus radius, with resonant surface indicated by vertical line

Fig.3.14.a

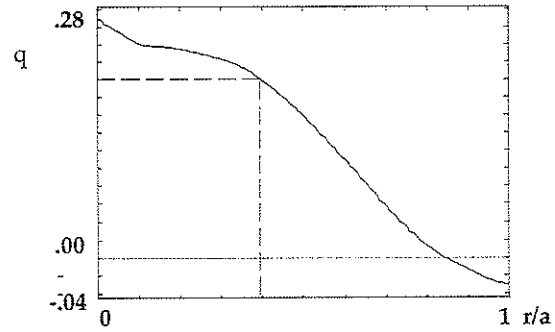

Fig.3.14.b

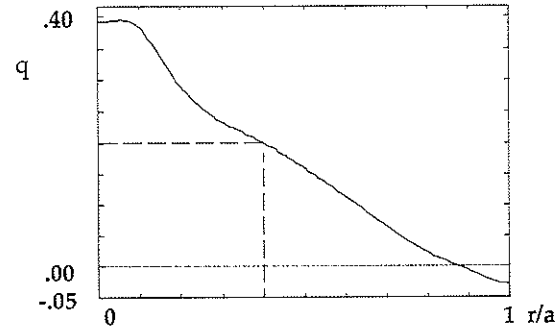

Fig.3.14.c

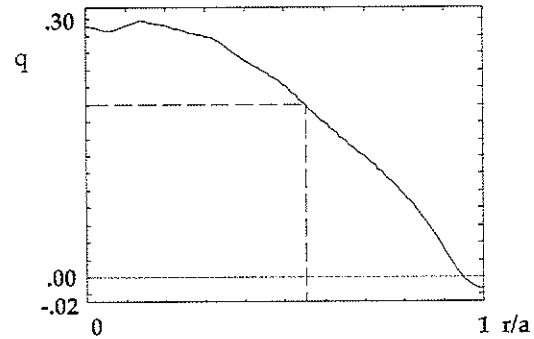

Fig.3.14: Safety factor q versus r; dashed lines indicate q=.20 and the (1,-5) resonant surface.
(a) conducting shell
(b) resistive shell with (1,-5) and (1,-7) feedback
(c) resistive shell without feedback

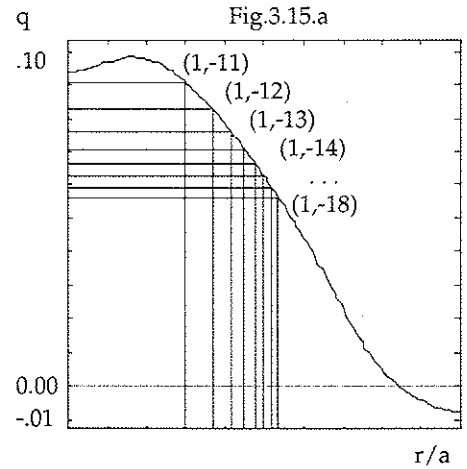

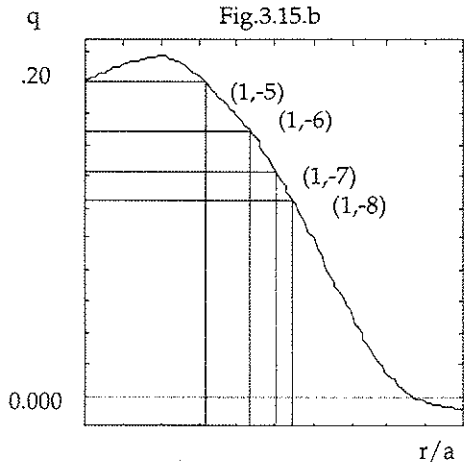

Fig. 3.15: Safety factor profiles with resonant surfaces of dominant tearing modes for
a) large aspect-ratio (R/a=6.0) steady state; b) small aspect-ratio (R/a=2.5) steady state

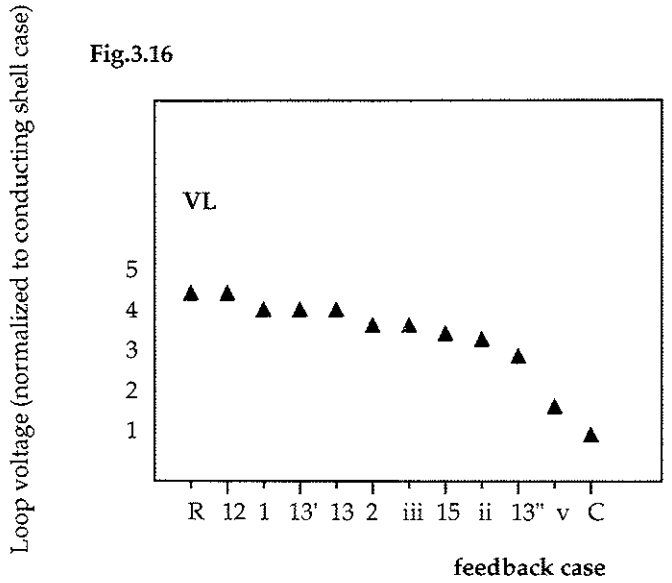

Fig.3.16: Loop voltage (normalized to conducting shell case) for different R/a=6.0 feedback cases:
R: resistive shell; **12**: resistive shell with (1,-12) feedback; **1**: resistive shell with (0,1) feedback; **13'**: resistive shell with (0,1)&(1,-13) feedback; **13**: resistive shell with (1,-13) feedback; **2**: resistive shell with (0,2) feedback; **iii**: resistive shell with (1,-11)&(1,-13)&(1,-15) feedback; **15**: resistive shell with (1,-15) feedback; **ii**: resistive shell with (1,-11)&(1,-15) feedback; **13"**: resistive shell with (1,-13)&(0,2) feedback; **v**: resistive shell with (1,-11)&(1,-12)&(1,-13)&(1,-14)&(1,-15) feedback; **C**: conducting shell (all modes stabilized)

Fig.3.17.a

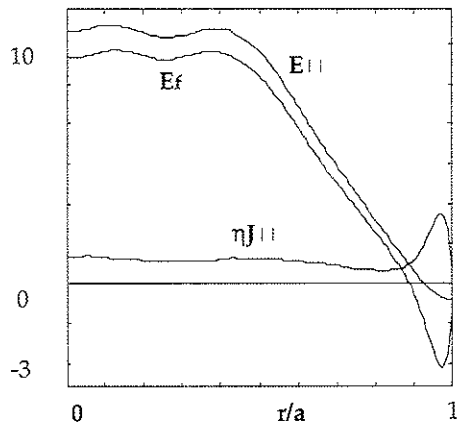

Fig.3.17.b

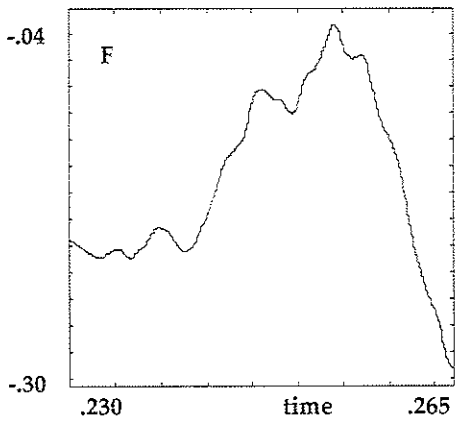

Fig.3.17. Resistive shell with feedback on (m=1,n=2) mode: a) Radial profiles of total parallel electric field $E_{||}=Ef+\eta J_{||}$, Ef, and ηJ where parallel fluctuation-induced electric field $Ef = -\langle vxb\rangle \cdot B/|B|$; b) Reversal parameter $F=Bz(a)/\langle B\rangle$ versus time

References

1 Y.L. Ho and S.C.Prager, Phys. Fluids B **3** (1991) 3099

2 A.Y. Aydemir, D.C. Barnes, E.J. Caramana, A.A. Mirin, R.A. Nebel, D.D. Schnack, A.G. Sgro, Phys. Fluids **28** (1985) 898

3 P.Kirby, Phys.Fluids **31** (1988) 625

4 Dan den Hartog, private communication, University of Wisconsin, Madison, Wisconsin, 1992

5 D.D. Schnack

6 K.L.Sidikman, PhD Thesis, University of Wisconsin-Madison, DOE/ER/53212-157 (1990)

7 J.P. Freidberg, Ideal Magnetohydrodynamics, Plenum Press, 1987, p.142

8 J.D Jackson, Classical Electrodynamics, Wiley 1975, New York, p.20

9 B. Alper, M.K. Bevir, H.A.B. Bodin, C.A. Bunting, P.G. Carolan, J. Cunnane, D.E. Evans, C.G. Gimblett, R.J. Hayden, T.C. Hender, A. Lazaros, R.W. Moses, A.A. Newton, P.G. Noonan, R. Paccagnella, A. Patel, H.Y.W. Tsui, P.D. Wilcock, Plasma Phys. Controlled Fusion **31** (1989) 205

10 C.G. Gimblett, Proc.: Physics of Mirrors, Reversed Field Pinches and Compact Tori, Varenna, Vol.1 (1987) 241

11 B. Alper, M.K. Bevir, H.A.B. Bodin, C.A. Bunting, P.G. Carolan, J.A. Cunnane, D.E. Evans, C.G. Gimblett, R.J. La Haye, P. Martin, A.A. Newton, P.G. Noonan, A. Patel, S. Robertson, H.Y.W. Tsui, P.D. Wilcock, *Results from HBTX reversed field pinch with close and distant resistive shells*, in Controlled Fusion and Plasma Physics (Proc.16th Eur. Conf. Venice, 1989), Vol. 13B , Part II, European Physical Society (1989)

12 E.J. Nilles, Y.L. Ho, S.C. Prager, D.D. Schnack, Bull. APS Div. Plasma Phys. **34**(9) (1989) 8P22, p.2147

13 C.G. Gimblett and D.D. Schnack, *Simulation of the thin shell and*

secondary shell HBTX1C experiments, Science Applications International Corporation SAIC-91/1016:APPAT-140 (1991)

14 D.D. Schnack, E.J. Caramana, R A Nebel, Phys. Fluids **28** (1985), 321

15 J.A. Holmes, B.A. Carreras, T.C. Hender, H.R. Hicks, V.E. Lynch, An, Diamond, Phys. Fluids **28** (1985) 261

16 Y.L. Ho and S.C.Prager, Phys. Fluids B **3** (1991) 3099

CHAPTER 4.

NONZERO $B_r(a)$ FEEDBACK

4.1 INTRODUCTION

Two sets of questions motivated tests of feedback schemes with nonzero $B_r(m,n)|_a$. First, we must ask about consequences of using nonideal feedback coils since, experimentally, $B_r(m,n)|_a$ cannot be precisely nulled at all times. Second, we ask whether feedback can not just approach the conducting-shell case but actually improve on it. The first question is investigated by simulating resistive feedback coils in Section 4.2. Improvements over the conducting shell are attempted with active programming of edge fields in Section 4.3.

4.2 VARIABLE COIL RESISTIVITY

There are several senses in which experimental feedback schemes must differ from the computational scheme tested above. There will be time lags or phase shifts between sensing an edge field and nulling it, due to finite time-response of the feedback circuit. The amplitude of the resultant edge field will be zero only within the limits of accuracy of the sensing and nulling circuits. These sources of error can be exacerbated and

confounded by interactions between the feedback circuit and the circuits comprising the plasma, wall, and field coils. Questions of mutual inductance and circuit stability have been explored analytically[1] and experimentally[2], and work remains to be done in these areas.

We simulated the plasma's response to nonideal feedback by assigning a finite resistivity to the feedback coils. Resistive feedback coils imperfectly null the targeted $B_r(m,n)|_a$, at each instant in time, since a finite edge field can persist radially. Looking at it another way, resistive coils null the targeted $B_r(m,n)|_a$ but with a time lag on the order of the characteristic vertical field soak-in time τ_{fb} of the feedback coils. By the time the applied field is seen by the plasma, it has the wrong value to null $B_r(m,n)|_a$, which has evolved meanwhile.

Numerical implementation of resistive feedback coil boundary conditions is a hybrid between full resistive shell boundary conditions (applied to all modes)[3] and individual conducting coil boundary conditions (applied to selected modes) (Ch.3). Boundary conditions for a shell whose resistivity is characterized by τ_S, the vertical field soak-in time for the shell, are applied to all modes (App.3). B_r is matched[4] from edge plasma $B_r(a)$ to vacuum solutions on the other side of the resistive shell with soak-in time τ_S by $\frac{\partial b_r}{\partial t} = \frac{a}{\tau_s}\left[\frac{\partial b_r}{\partial r}\right]_a$. This boundary condition is then superseded for feedback-targeted modes (m,n) by a similar matching from the plasma edge through a feedback coil of helicity (m,n) and

effective soak-in time τ_{fb}, to the vacuum B_r, by $\frac{\partial b_r}{\partial t} = \frac{a}{\tau_{fb}}\left[\frac{\partial b_r}{\partial r}\right]_a$ where [ ] indicates the jump condition across the stabilizing resistive coil. In both cases, the vacuum B_r is obtained from Bessel function solutions to $\nabla x \mathbf{b}=0$.

4.2 a Linear tests of resistive feedback coils

The resistive coil feedback scheme was first tested linearly (with frozen mean fields and no mode interaction) by setting coil τ_{fb} to each value used for τ_S in conducting and resistive shell cases. A long shell time ($\tau_S = 1000\ \tau_R$) approximates a perfectly conducting shell. Modes grow slowly in this reference case (Fig.4.1a). We then choose a short shell time $\tau_S = 0.032\ \tau_R$ to characterizes a shell so resistive that a typical run can span several shell times. (Typically, a conducting-shell steady state is given resistive-shell boundary conditions at $t_0=.180\tau_R$; then the plasma evolves in a resistive shell to $t_1=.212\tau_R = t_0 + \tau_S$, $t_2=.244= t_0 + 2\tau_S$, etc.) Rapid linear growth in the resistive shell reference case is evident in Fig.4.1b.

First, we superpose a conducting coil on the resistive shell, not by setting $B_r(m,n)|_a= 0$ but by choosing $\tau_{fb}= 1000\ \tau_R$for the (m,n) coil. In this test, the targeted mode's linear growth precisely matches its rate with a full conducting shell ($\tau_S =1000\tau_R$) while other modes grow as in a full resistive shell (Fig.4.1.b). With a resistive coil on resistive shell, ($\tau_{fb}(m,n) = \tau_S = 0.032\tau_R$), all modal linear growth rates match the pure resistive shell case

(Fig.4.2.i). Having established the reliability of our resistive coil scheme at the extremes of high and low conductivity, we investigate effects of varying the coil resistance between these extremes.

Progressively more resistive coils stabilize the targeted mode over several decades of τ_{fb}, until $\tau_{fb} \sim 1.0\tau_R$ (Fig.4.2.ii). At this point, coil resistivity begins to noticeably compromise stabilization capacities of the feedback circuit. While linear growth rates are negative in the "conducting" coil case ($\tau_{fb} = 1000\tau_R$), growth rates rise toward zero when $\tau_{fb} = 1.0\tau_R$. When the characteristic time constant of feedback coils is on the order of the resistive diffusion time, the dominant tearing modes are only marginally linearly stable.

4.2 b Nonlinear tests of resistive feedback coils

After subjection to a series of linear tests, the resistive coil feedback boundary conditions are applied to nonlinearly evolving RFPs for several values of τ_{fb}. When allowed to interact with each other and to modify the equilibrium, dynamo modes grow almost as quickly with slightly resistive feedback coils ($\tau_{fb} = 100\ \tau_R$) as with a full resistive shell of $\tau_S = 0.032\ \tau_R$, as seen in Fig.4.3. However, V_L saturates at less than twice the conducting-shell level with resistive coils (Fig.4.4), while V_L continues to grow without feedback, due to modified E_F profiles as seen in Chapter 3 .

4.3 Δ' profile modification

4.3.1 Introduction

Linear growth of tearing modes is known to be driven by discontinuities in the slope of B_r at the resonant surface ($r=r_s$) of the mode. The discontinuity is described by the logarithmic derivative $\Delta' = \frac{\psi'_+ + \psi'_-}{\psi'_{rs}}$, where $B_r = (\nabla\psi)_\theta = im\psi$ and subscripts indicate flux function values at, or on either side of, the resonant surface of a given mode (m,n). Analytically, the linear[5] growth rate is found to be proportional to $(\Delta')^{4/5}$. Nonlinear growth[6] to amplitudes of order $(\tau_A/\tau_R)^{4/5}$ proceeds as t^2. In an effort to provide more active control of field profiles, the example of previous work[7] is followed. The approach is to force edge B_r to have the opposite sign of $B_r(r_s)$, in order to smooth out discontinuities in the flux function at the resonant surface. We advance the code linearly and search for the ratio $f = B_r(r_s)/B_r(a)$ which most nearly corrects for discontinuities in B_r', reducing $\Delta'(r_s)$ and the growth rate of the targeted mode. (cf Fig.2 from Ref.7).

4.3.2 Abrupt $B_r(a) = f\,B_r(r_s)$ application

4.3.2 a Linear tests

We apply $B_r(a) = f\,B_r(r_s)$ to (m,n)=(1,-5) for various values of f. Linear tests with this scheme reveal that there is a range for $f<0$ in which

modes are temporarily stabilized, but that a phase-flip instability is induced at large f: the mode shifts so that it is driven, not stabilized, by the applied edge field. With f=-0.1, mode amplitudes are reduced below resistive-shell levels, though they are higher than conducting-shell levels (Fig.4.5a). While this is partly due to decreasing the driving term $\Delta'(r_s)$, it should be noted that the absolute value of $B_r(a)$ is decreased by $|f|<1$. This can mimic effects of high conductivity feedback coils. Ordinarily, $B_r(a)/B_r(r_s)>25\%$ in nonlinear resistive shell computations (Fig.4.6) without feedback.

Applying a large negative $B_r(a)$, when $B_r(r_s)>0$, leads to an instability in which $B_r<0$ throughout the plasma, called the phase flip instability. When feedback is strengthened to f=-1.0, the phase flip instability appears, increasing the magnetic energy in the targeted mode beyond its resistive-shell levels (Fig.4.5b). The deep negative edge field initially drags $B_r(r_s)$ to lower levels, decreasing the fluctuation amplitude temporarily. However, the stretched field line snaps down (Fig.4.7), propelling $Br(r_s)$ to a large negative value, where high mode amplitude in a flipped state is now consistent with the negative $B_r(a)$. The mode grows out of phase with its original profile until feedback changes the sign of the edge field and the process reverses. The net effect is to ratchet up the mode amplitude, which oscillates about a growing level. In addition, the abrupt application of this extreme boundary condition drives the mode initially to an amplitude orders of magnitude above its initial resistive-shell level (Fig.4.7.a).

4.3.2 b Nonlinear tests

Since $Br(m,n)|a=0$ feedback proved most effective when applied to several nonlinearly interacting candidate dynamo modes simultaneously, we apply $B_r(a) = f \cdot B_r(r_s)$ to m=1, n=-5, -6, and -7 in this series of tests. At all values of f tested, $B_r(a) = f \cdot B_r(r_s)$ drives the RFP nonlinearly unstable within .001 τ_R by exciting high amplitude fluctuations from which the feedback scheme cannot rescue it. Edge E_F grows positive, destroying reversal, and loop voltage skyrockets in a vain attempt to maintain plasma current.

This feedback scheme is clearly of limited value in nonlinear cases. Potentially more useful schemes might impose edge fields proportional not only to the amplitude but also to the time derivatives of the signal (in this case, $B_r(a)$). Analysis of this problem requires calculation of transfer functions describing the plasma circuit, which is tractable only in the linear case. In experimental RFPs, where nonlinear dynamics dominate, transfer functions are undefined. Two other improvements on this scheme suggest themselves. First, feedback on the mode velocity may provide a more sensitive tuning parameter, since changes in v_r precede the phase flip. Second, since abrupt application of the $B_r(a)=f\,B_r(r_s)$ boundary condition initially jars the system into large fluctuations, dialing up this boundary condition slowly from zero may allow stabilization to take place nearly adiabatically. The latter method is investigated in the next section.

4.3.3 Rampup to $B_r(a) = f \cdot B_r(r_s)$

To avoid overdriving targeted modes with unusually large initial $B_r(a)$, we ramp up the feedback parameter f from 0 to its maximum specified (negative) value in about one shell time. The initial feedback boundary conditions (f=0) are equivalent to those of a conducting coil. As f increases, coil conductivity is gradually relaxed and response of the feedback circuit to the plasma's $B_r(r_s)$ strengthens, until the full feedback response at f_{max} is established.

4.3.3.a Linear tests

When f is ramped from 0 to -0.1 on (1,-5), the mode's linear growth rate approaches zero (Fig.4.8), compared to continued growth in the resistive shell case. The phase flip instability is avoided, but the modal magnetic energy saturates at a higher level than in either the conducting-shell or the resistive-shell cases.

4.3.3.b Nonlinear tests

Unlike nonlinear runs with abruptly applied $B_r(a) = f \cdot B_r(r_s)$, rampup of this boundary condition on m=1, n=-5,-6,-7 does not lead to rapid fluctuation growth and run termination. Modal magnetic energies are slightly higher than levels with $B_r(a)$=0 feedback on these three modes

(Fig.4.9), and VL oscillates about a comparable (or perhaps slightly lower) average value (Fig.4.10). No phase flip instability is driven. The driving term and the (linear) island width

$$w = 4r_s \sqrt{\frac{|b_r(r_s)|}{B_\theta(r_s)} \left[\frac{r_s}{a} \left| n \frac{\partial q}{\partial (r/a)} \right|_{r_s} \right]^{-1}}$$

are both decreased. While the goal of improvement on the conducting shell case has not been achieved, we have demonstrated that this more realistic active feedback scheme can very closely approach results using the more idealized $B_r(a)$=0 scheme. This is somewhat surprising, since this scheme targets a linear driving term but nonlinear mode interactions are very strong.

Note: Plasma parameters such as steady-state V_L differ from $B_r(a)$=0 data presented in Chapter 3 because the initialization from which the nonlinear tests in this section were restarted differs from the initialization used for runs in Ch.3. The initialization of this chapter was generated by running through a resistive-shell phase before application of feedback boundary conditions; the initialization of Ch.3 came from a purely conducting-shell run. Therefore, loop voltage values are higher before the application of feedback.

4.4 Summary of nonzero $B_r(m,n)|_a$ results

These preliminary tests of simple nonideal feedback schemes provide a starting point for further investigations. We have found that linear tests can help one home in on ranges of feedback parameters which may prove useful in fully nonlinear tests of a new feedback scheme. (Quasilinear tests, in which fluctuations can modify equilibrium profiles but do not interact with each other, could be a useful intermediate step.) However, feedback schemes which appear promising linearly often fail, nonlinearly, as interaction between fluctuations modify feedback effects in unpredictable ways.

Tests of resistive feedback coils yield information on effects of feedback with finite effective soak-in time τ_{fb}, or imperfect nulling of $B_r(m,n)|_a$. Coils require $\tau_{fb} \geq 100\tau_R$ in order to reduce loop voltage toward conducting shell V_L.

Active edge feedback in response to values of Br at a mode resonant surface drives a phase flip instability if applied too aggressively. Gentle rampup to a carefully chosen proportionality between $B_r(r_s)/B_r(a)$ can reduce V_L toward the conducting shell value. Further fine-tuning of this scheme holds potential for improvements over conducting-shell parameters in future investigations.

Elsewhere[8], an algorithm modeling nonideal feedback on edge $B_r(m,n)|_a$ in response to sensed $B_r(m,n)|_a$ has been tested:

$$\frac{\partial b_r}{\partial t} = -\frac{a}{\tau_{fb}}\left\{\left[\frac{\partial b_r}{\partial r}\right]_a + \min\left(\frac{c_1^4}{(c_1^2-b_r^2)^2}, 1.e^{10}\right)\frac{b_r}{c_2}\right\}$$

where [ ] indicates the jump condition across the resistive shell, here equivalent to a resistive shell with a negative diffusion coefficient; and min( ) serves as an anti-runaway damping term: c_2=clamping term and c_1=damping term.

This scheme can also induce phase-flip instabilities and rapid fluctuation growth. With careful choice of parameters τ_{fb}, c_1 and c_2, it is possible to reduce magnetic fluctuations below levels found in the conducting-wall RFP, in quasilinear tests. In full nonlinear tests, however, the targeted mode continues to grow and the scheme fails to improve on the conducting shell case. Even if fine-tuning of this more sophisticated scheme cannot reduce V_L below the conducting-shell level, it demonstrates the potential feasibility of a more physically realistic feedback circuit based on sensing of edge fluctuations.[2]

Fig.4.1.a

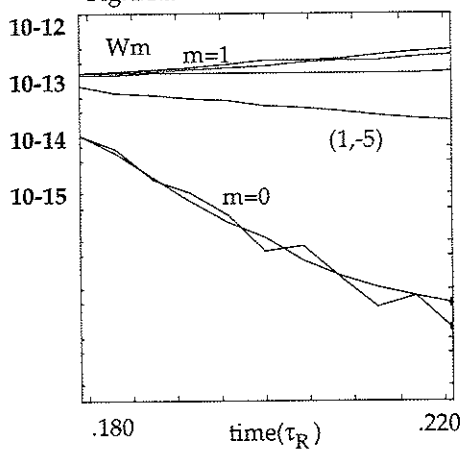

Fig.4.1.b

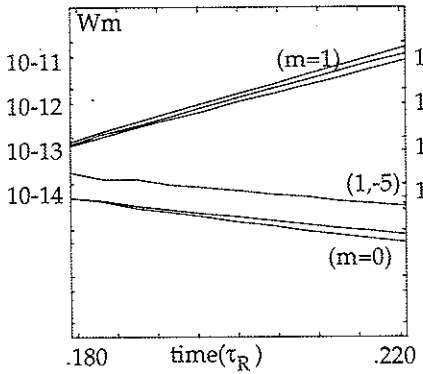

Fig.4.1.c

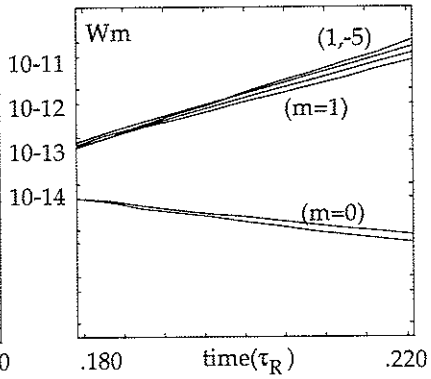

Fig.4.1: Modal magnetic energies versus time for linear runs in:
(a) conducting shell (τs = 1000 τR)
(b) resistive shell with conducting feedback coils for (m,n) = (1,-5)
(c) resistive shell without feedback (τs = .032 τR)

The "m=1" modes include -n = 4, 6, 7. The "m=0" modes include n=1,2.

Fig.4.2

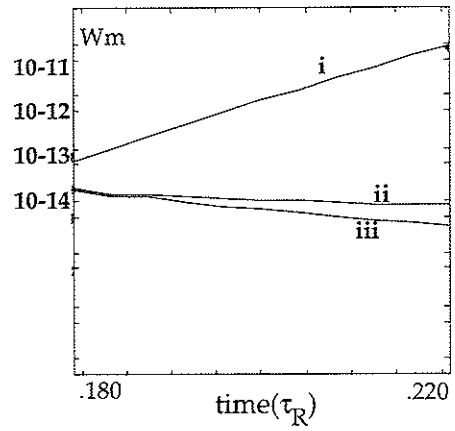

Fig.4.2: Magnetic energy of (1,-5) vs. time with linear stabilization by coils of varying resistivity:
(i) τfb=0.032 τR: high resistance coil, equivalent to no feedback
(ii) tfb = 1.0 τR: resistive coil
(iii) tfb = 1000 τR: low resistance coil, equivalent to ideal feedback

Fig.4.3.a Wm

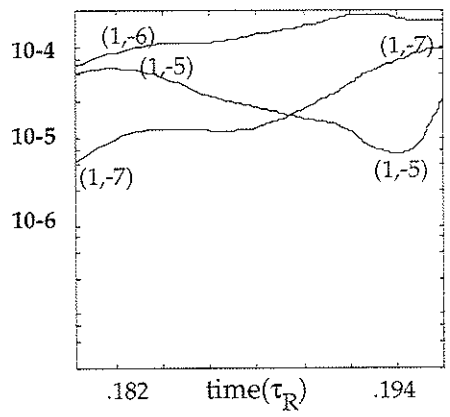

Fig.4.3.b Wm

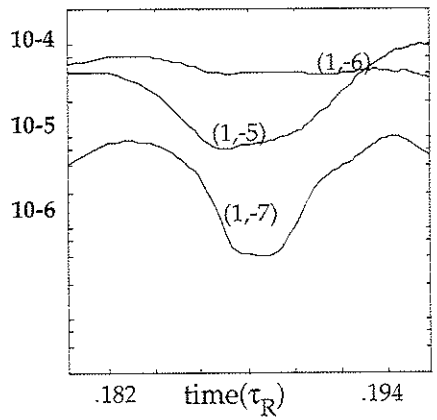

Fig.4.3: Modal magnetic energy versus time for nonlinear resistive shell runs (a) without feedback, and (b) with resistive feedback coils (tfb = 100 τ_R) for m=1, n=-5,-6,-7

Fig.4.4.a: no feedback

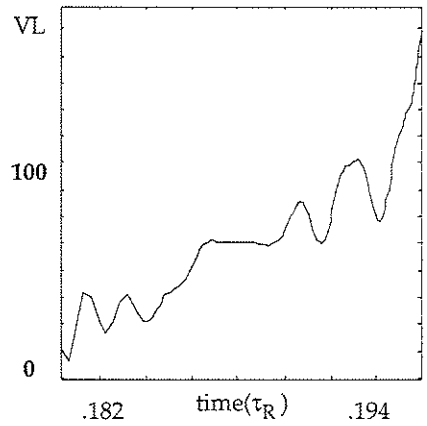

Fig.4.4.b: resistive coils

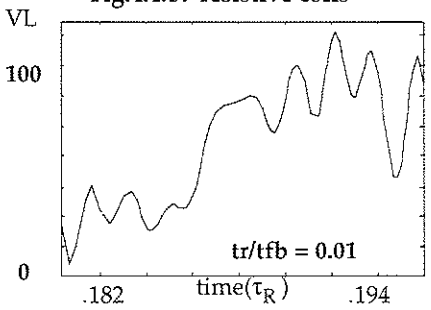

Fig.4.4: Loop voltage versus time for nonlinear runs with resistive shell:
(a) without feedback
(b) with resistive feedback coils on m=1, n=-5,-6,-7

FIG 4.5a: f=-0.1

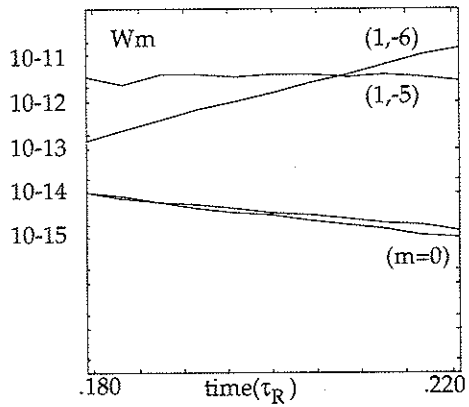

FIG 4.5b: f=-1.0

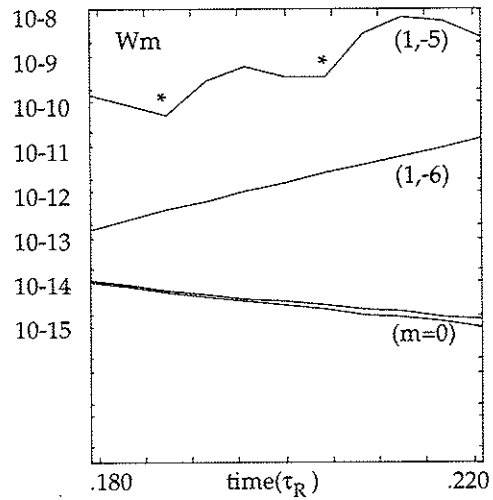

Fig.4.5: Modal magnetic energy spectra versus time for linear feedback on (1,-5): br(a) = -f br(rs) (phase flips at *):

(a) f=-0.1 reduces amplitude and growth rate of (1,-5)

(b) f=-1.0 induces phase flip and enhances growth of (1,-5)

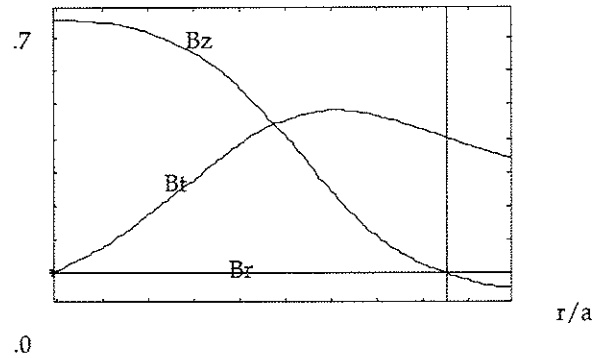

Fig.4.6.a: Axisymmetric (0,0) magnetic field component profiles with resistive shell after evolution for one half of one shell time (from t=.180 tR to t=.196 tR).

Fig.4.6.b

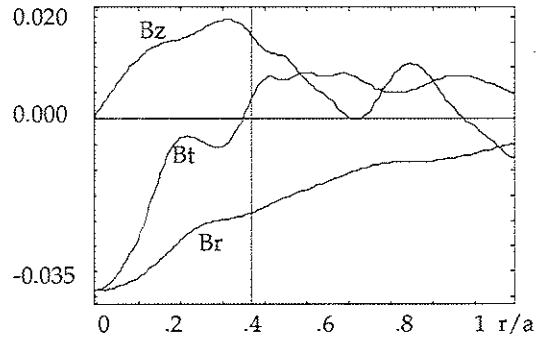

Fig.4.6.c

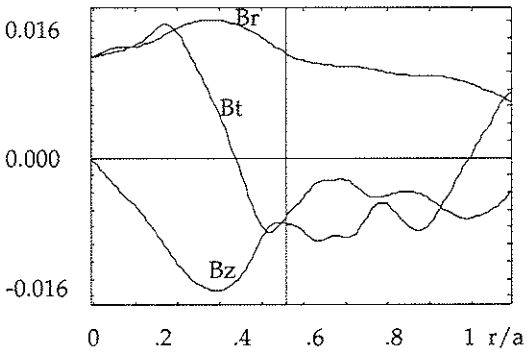

Fig.4.6.d

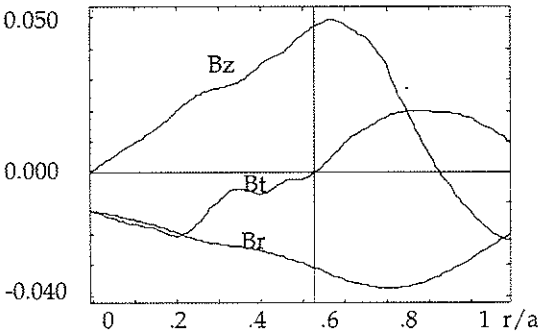

Fig.4.6: Magnetic field fluctuations profiles with resistive shell after evolution for one half of one shell time
(**b**) (m,n) = (1,-4); (**c**) (m,n) = (1,-5); (**d**) (m,n) = (1,-6)

Fig.4.7.a

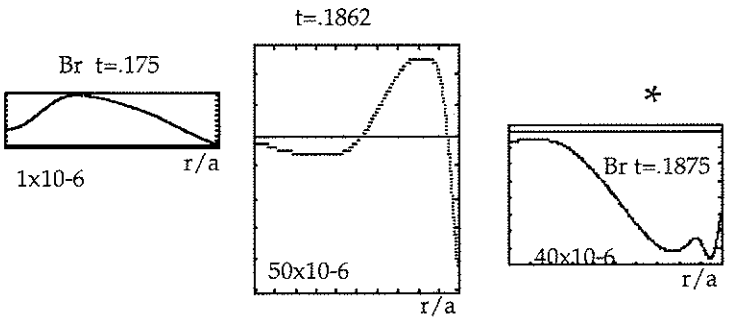

Fig.4.7.b

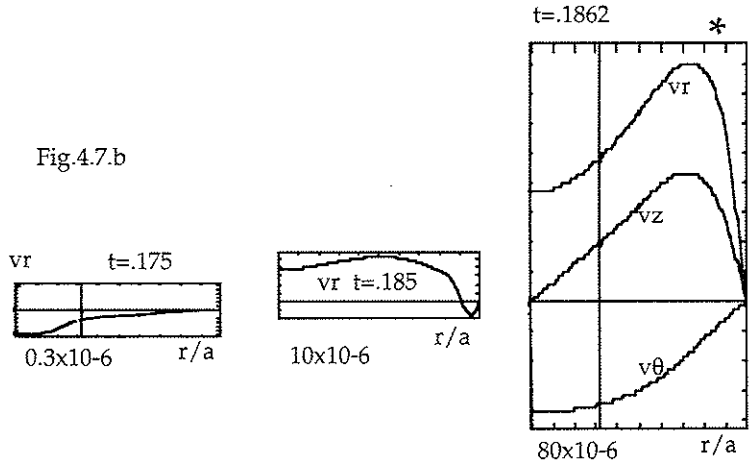

Figs.4.7: Velocity vr sign change at edge predicts phase flip (at *) in Br(r)

(a) Magnetic field profiles before and during phase flip
(b) Velocity profiles before and during phase flip
(only roughly to scale)

Fig.4.8

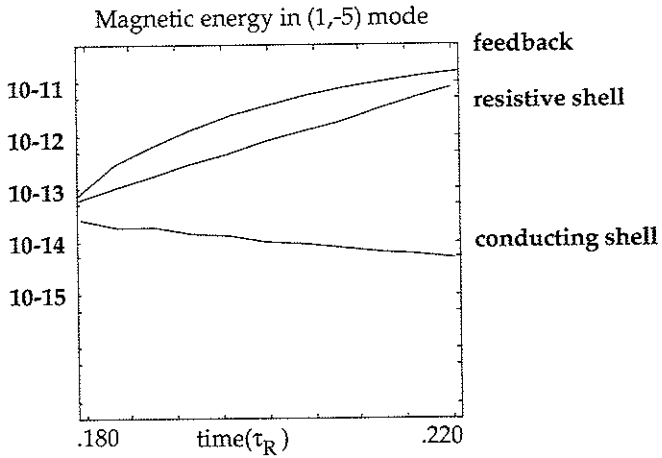

Fig.4.8: Magnetic energy versus time for linear feedback on (1,-5). ramping f from 0 to 0.1.

Fig.4.9.a

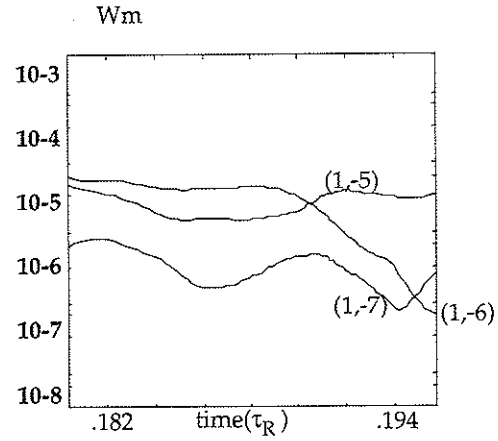

Fig.4.9.b

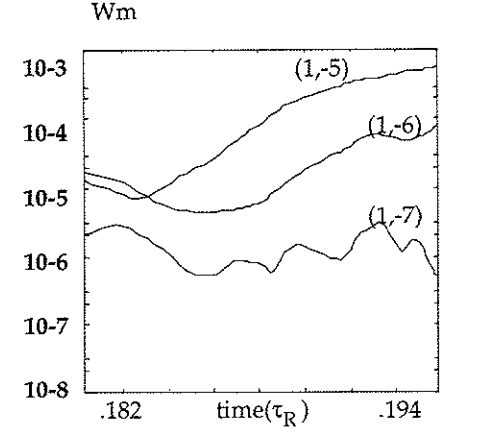

Fig.4.9: Modal magnetic energy versus time for nonlinear run with feedback on modes m=1, n=-5,-6,-7
(a) perfectly conducting feedback coils
(b) ramping f from 0 to -0.1.

Fig.4.10.a

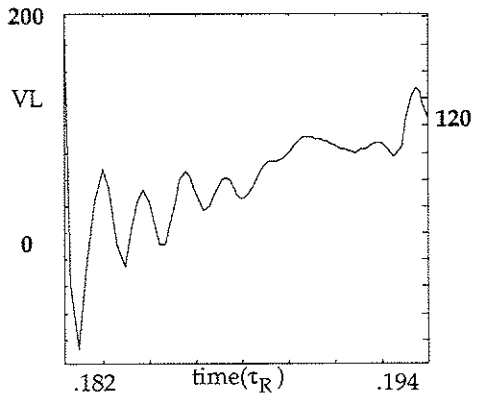

Fig.4.10.b

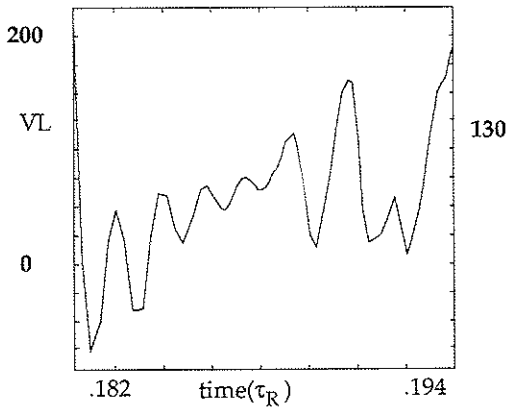

Fig.4.10: Loop voltage VL versus time for nonlinear run with feedback on modes m=1, n=-5,-6,-7
(a) perfectly conducting feedback coils
(b) ramping f from 0 to -0.1.

References

1 C.M. Bishop, *An Intelligent Shell for the Toroidal Pinch*, Culham Laboratory report CLM-P845 (1988)

2 C.L.Platt, S.H. Robertson, IEEE Transactions on Plasma Science **19** (1991) 954

3 Y.L. Ho, PhD Thesis, University of Wisconsin-Madison, DOE/ER/53212-131

4 ibid

5 R.B. White, in Handbook of Plasma Physics, Vol.1, edited by A.A. Galeev and R.N. Sudan (North-Holland, New York, 1983) 622

6 PH Rutherford, Phys. Fluids **16** (Nov.1973) 1903

7 D.A. Monticello, R.B. White, and M.N. Rosenbluth, *Feedback stabilization of magnetic islands in tokamaks*, 7th IAEA, Innsbruck **1** (1978) 605 [IAEA-CN-37/K-3]

8 Y.L. Ho, US-Japan RFP Workshop on Anomalous Ion Heating and Related Topics University of Wisconsin, Madison, Wisconsin (2-4 March 1992)

CHAPTER 5

ROTATION OF PLASMA/WALL AND MODES

5.1 Introduction

It has been observed that when tearing modes in RFPs phase-lock to each other[1,2] or in space (e.g. to a shell gap), [3,4] their growth rates increase, often leading to early termination. Bulk plasma rotation inhibits growth of tearing modes for at least two reasons. First, modes at rest in the frame of a spinning plasma see an effectively more highly-conducting shell, imposing lower limits on Br(a). Second, if a rotating mode tries to lock (cease rotating) due to stationary field errors, stabilizing viscous drag forces arise between the deccelerating mode and the rotating bulk plasma surrounding it. These forces tend to inhibit growth of the mode. Therefore, causing either rotation of the bulk plasma with respect to the shell or rotation of tearing modes with respect to the bulk plasma may be a useful means of feedback stabilization.

In this chapter, we present work in progress investigating the efficacy of rotation as a means of stabilizing tearing modes. In Section 5.2, we rotate the resistive shell at various accelerations to various maximum velocities, first in linear then in nonlinear tests. In Section 5.3, we propose rotating individual modes with respect to the plasma, in a scheme which has yet to be tested.

5.2 Spinning wall/plasma

In these tests, the resistive shell which bounds the RFP is accelerated from rest (spun up) to various final constant rates in the axial and poloidal directions, to model bulk plasma rotation in the opposite direction of shell spinning. Shell spinning has also been proposed as a physically feasible option, in the form of a rotating liquid metal blanket[5,6] between confining resistive shells. Toroidal and/or poloidal rotation is implemented numerically by specifying mean $v_z(0,0)$ and/or $v_\theta(0,0)$ at the wall and including these velocities in the convective derivative term for the magnetic field perturbation evolution, at the boundary, as detailed in Appendix 3. Rates of spin up are specified independently by increasing v_z and v_θ at each time-step, before they are used in the boundary condition.

For this cylindrical model, toroidal rotation of the shell reduces to relative linear motion between the shell and the bulk plasma. Therefore, shell rotation with $+v_z$ is equivalent to plasma rotation with $-v_z$. However, poloidal shell rotation with $+v_\theta$ is not equivalent to plasma rotation with $-v_\theta$. In a moving plasma, Coriolus effects will add a poloidal component to perpendicular motion: radial paths will spiral and axial paths will become helical. In addition, a rotating plasma with mass density ρ will experience a $\rho v^2/r$ outward force. (Similarly, in a truly toroidal geometry, shell rotation with $+v_z$ is is not equivalent to plasma rotation with $-v_z$. These discrepancies are not addressed in our tests.

The results below are briefly summarized. In linear tests, mode growth decreases as rotation rate increases and as spin-up rate increases, approaching the conducting-shell approximation at very high rates. In nonlinear tests, rotation at realistically low rates has a negligible effect on plasma parameters. Nonlinear tests of high rotation rates are beyond the scope of this thesis.

5.2 a Linear tests

Fig.5.1 **m=1 magnetic energies versus time**

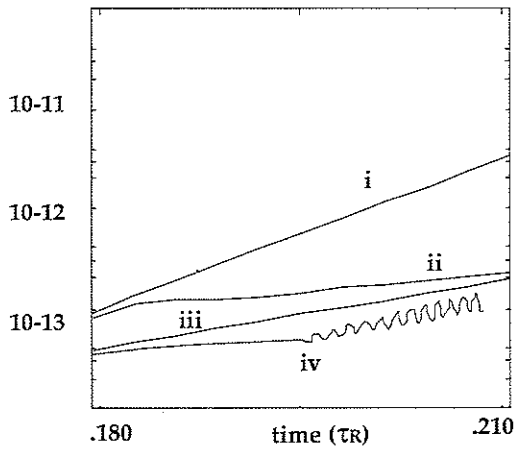

Fig.5.1: Magnetic energies versus time for four cases:
i: resistive shell without rotation
ii: resistive shell accelerating at $10v_A/\tau_R$
iii: conducting shell without rotation
iv: resistive shell accelerating at $100v_A/\tau_R$
(oscillations onset at velocities near v_A)

Linear tests of the effectiveness of relative motion between the bulk plasma and the resistive shell, spinning the shell up at a rate of $dv_S/dt = 10v_A/\tau_R$ holds magnetic fluctuations in a resistive shell of τ_S=.032 τ_R nearly as low as in a conducting shell (Fig.5.1, curve ii). Spinning the shell up faster, at $dv_S/dt = 100v_A/\tau_R$, holds fluctuations near the "conducting shell" (τ_S=1000τ_R) levels (Fig.5.1.iv), which are only an approximation to a true conducting shell (τ_S=infinity).

5.2 b Nonlinear tests

Plasma rotations tend to be characterized by the diamagnetic drift velocity. For example, in the MST experiment, assuming[7] $n(0)\sim10^{13}$ cm^{-3}, T(0)~400eV, <BT>~1.2 kG, and Z=2, the diamagnetic drift velocity $v_D = -\nabla P \times B/qnB^2 \approx 7\times10^3$ m/s. The diamagnetic drift speed and direction varies with radius, from poloidal on axis to toroidal at the reversal surface, and helical elsewhere. A diamagnetic drift velocity cannot be defined for the DEBS code, which has no pressure gradient. Computational speeds are referenced to the Alfven speed, $v_A = B/\sqrt{4\pi n_i m_i}$, which is about 6×10^5 m/s in the MST experiment. It is observed that helical modes in MST rotate at about $v_Z\sim7.5\times10^4$ m/s ~ $10v_D$. Rotating modes can lock to the wall within 0.1 ms after a sawtooth crash, when the bulk plasma shifts inward in major radius, sampling a higher field error at the poloidal gap; thereafter, modes can grow quickly.[8]

Effects of a spinning shell on nonlinear RFP evolution have been investigated for a range of maximum shell speeds v_z and v_θ and for a range of acceleration rates dv_z/dt and dv_θ/dt to these maxima. Poloidal and toroidal rotation speeds were each varied from $4x10^{-5}$ to $4x10^{-3}$ v_A, and each value was approached at accelerations between 1-100 v_A/τ_R. These would correspond to .approximately .0035-.35 v_D in an RFP such as MST.

Shell rotation at velocities below $4x10^{-3}$ v_A yields no significant drop in loop voltage or modal magnetic energies. This is not surprising, since experimental RFPs are observed to benefit from rotations larger than those tested. Peak rotations in these tests remain far lower than rotation rates reached in linear tests. Numerical instabilities of undetermined origin preclude modeling of rotations above 10^{-2} v_A. Nonlinear tests of plasma/shell rotation are inconclusive and should be continued.

5.3 Spinning individual modes

It has been observed in Tokamak and RFP experiments that spinning of individual modes with respect to tthe bulk plasma inhibits their rapid growth. Numerical computations[9] have quantified the minimum perturbation field necessary to "lock" a mode to an error field while embedded in a rotating plasma. The converse problem, to find the reduction in growth rate of a locked mode if it is made to rotate, has yet to be solved for either the Tokamak or the RFP. We have begun an analysis

of this problem, as detailed in Appendix 3. We propose to use edge fields to drag islands with respect to the plasma. Flow around the islands may reduce their size and their growth rate, as seen experimentally. Modeling and testing of a feedback scheme based on mode rotation induced by helical feedback coils remains to be completed.

References

1 T. Tamano, W.D. Bard, R.J. LaHaye, M.J. Schaffer. P.L. Taylor, Phys. Rev. Lett **59** (1987) 1444

2 R.J. LaHaye, P.S. Lee, M. Schaffer, T. Tamano, P.L. Taylor, Nucl. Fusion **28** (1988) 918

3 B. Alper, M.K. Bevir, H.A.B. Bodin, C.A. Bunting, P.G. Carolan, J. Cunnane, D.E. Evans, C.G. Gimblett, R.J. Hayden, T.C. Hender, A. Lazaros, R.W. Moses, A.A. Newton, P.G. Noonan, R. Paccagnella, A. Patel, H.Y.W. Tsui, P.D. Wilcock, Plasma Phys. Controlled Fusion **31** (1989) 205

4 A.F. Almagri, S. Assadi, S.C. Prager, J.S. Sarff, D.W. Kerst, *Locked modes and magnetic field errors in MST*, accepted for publication, Phys. Fluids B (1992)

5 T.C. Hender, C.G. Gimblett, D.C. Robinson, 13th European Conf on Controlled Fusion and Plasma Heating, Schliersee **1** (1985) 61

6 C.G. Gimblett. Nucl. Fusion 31 (1989)

7 S.C. Prager. et al., Phys. Fluids B **2** (1990) 1367

8 A. Almagri and J. Sarff, private communication, University of Wisconsin-Madison, 1992

9 R. Fitzpatrick and T.C. Hender, Phys. Fluids B **3** (1991) 644

CHAPTER 6

CONCLUSION

The growth of tearing modes in resistive shell Reversed Field Pinch experiments can degrade plasma parameters and lead to shortened plasma discharge durations. This thesis does not directly address questions of transport but uses insights from Ohm's law to tailor field profiles and control plasma parameters. Several schemes for edge feedback stabilization of internal tearing modes have been tested numerically. A computer program for solving the nonlinear, resistive, compressible, zero-beta magnetohydrodynamic equations in three dimensions has been modified for this purpose.

The most completely tested feedback scheme, presented in Chapter 3, nulls the radial magnetic field at a resistive shell, in helical patterns resonant with modes targeted for feedback. The effectiveness of this scheme lies in its ability to modify profiles of the fluctuation-induced electric field. The significance of this field in RFP dynamics has become increasingly clear in the decade since it was first proposed as the source of the RFP dyamo. Our investigations suggest that the shape of the fluctuation-induced electric field for just the few dominant resistive tearing modes largely determines global variables in the RFP. Negative

poloidal edge field drives the currents which provide reversal and sustain the mean flux; positive axial field can oppose the global thermal instability, but large axial field demands high loop voltage to sustain plasma current.

We find that stabilization of the highest-amplitude tearing mode fluctuations, approximately 2R/a in number, can decrease loop voltage and extend plasma discharge durations. Suppression of these modes does not suppress the RFP dynamo, because neighboring fluctuations evolve nonlinearly into dynamo mode form. Quasilinear interactions modify mean magnetic field and current profiles such as to reduce driving terms. This leads to an overall decrease in fluctuation amplitudes, and, more importantly, to a reshaping of the largest modal components of the fluctuation-induced electric field. Corresponding changes in the safety factor profile shift modal resonant surfaces radially inward. Experimentally, this could reduce plasma-wall interactions, resistivity, and transport.

We propose a physical mechanism by which external coils stabilize internal modes in Chapter 3, and predict requirements and effects of applying feedback stabilization to RFPs such as those in existence when this work was begun. A limited comparison with experiment is reported. In the light of evidence that feedback stabilization of resistive shell modes can restore RFP parameters to nearly their conducting-shell levels, further experimental tests of edge feedback and of RFP dynamo and transport dynamics are encouraged.

We have begun exploring alternative feedback schemes, including less effective methods with resistive instead of conducting windings, and potentially more effective methods with actively programmed boundary conditions (Chapter 4). In the former set of investigations, we find that imperfect nulling of the edge radial field suppresses targeted modes less completely, and quantify the required conductivity of feedback coils. In the latter set, we attempt to improve over conducting shell plasma parameters. Actively varying the edge radial field in response to mode amplitudes at the edge or inside the plasma yields mixed results. Most recently (Chapter 5), we find bulk plasma rotation a potentially useful method of stabilizing tearing modes; however, more work needs to be done to quantify minimum effective spin and acceleration rates in nonlinear RFPs. Finally, we sketch out an approach to modeling rotation of individual modes, to be induced by feedback coils. This last scheme has not yet been modeled.

This work has been supported by the U.S. Department of Energy.

APPENDIX 1

GENERATION OF MEAN ELECTRIC FIELD BY FLUCTUATIONS IN VELOCITY AND MAGNETIC FIELD[1]

Velocity and magnetic fields V and **B** may be written in terms of mean fields $\mathbf{V_0}$ and $\mathbf{B_0}$ and fluctuations **v** and **b**:

$$\mathbf{V}(\mathbf{r},t) = \mathbf{V_0}(\mathbf{r},t) + \mathbf{v}(\mathbf{r},t) \qquad \langle \mathbf{v} \rangle = 0 \qquad (1)$$

$$\mathbf{B}(\mathbf{r},t) = \mathbf{B_0}(\mathbf{r},t) + \mathbf{b}(\mathbf{r},t) \qquad \langle \mathbf{b} \rangle = 0 \qquad (2)$$

The mean, or global part of the field is defined as that which varies on a time scale T much longer than time scales characteristic of the fluctuations (t), and which exhibits structure on length scales L longer than fluctuation length scales l. Mean fields vary little over a characteristic dimension a of the system ($l << a << L$), and remain approximately constant over an intermediate timescale τ satisfying $t << \tau << T$. The ensemble average can be defined over time:

$$\langle \psi(\mathbf{r},t) \rangle_\tau = \frac{1}{2\tau} \int_{-\tau}^{\tau} \psi(\mathbf{r}, t+\tau') d\tau'$$

or over space:

$$\langle \psi(\mathbf{r},t) \rangle_a = \frac{1}{2\tau} \int_{|\xi|<a} \psi(\mathbf{r}+\xi, t) d^3\xi$$

Writing $\langle \mathbf{v} \rangle = 0$, for example, means that on time and length scales characteristic of the system, fluctuations average to zero. "The random ... field may be a turbulent ... field ... or it may consist of a random superposition of interacting wave motions."[2] The fluctuations treated pseudospectrally in this thesis are understood to take the latter form.

In the RFP, the characteristic length scale is a=minor radius and the characteristic timescale is $\tau = \tau_R^{3/5} \tau_A^{2/5}$ for resistive tearing.[3] Mean fields describe axisymmetric modes (m=0,n=0) with infinite poloidal and toroidal wavelengths; these typically evolve on resistive diffusion τ_R (millisecond) timescales. The longest wavelength RFP fluctuations of interest are helical magnetic islands with finite wavenumbers, typically $\frac{m}{n} \geq 2\frac{R}{a}$, with characteristic oscillations on τ_A (microsecond) timescales (megahertz frequencies). Smaller length scale fluctuations have shorter characteristic timescales, assuming group velocities are approximately constant across mode number .

Substituting (1) and (2) into

(3) $\frac{\partial \mathbf{B}}{\partial t} = -\nabla(\eta \mathbf{J} - \mathbf{v} \times \mathbf{B}) = \nabla \times (\mathbf{v} \times \mathbf{B}) + \lambda \nabla^2 \mathbf{B}$, where $\lambda = \frac{\eta}{\mu_0}$ is the magnetic diffusivity, yields an equation which can be separated into its first order and second order parts:

$$\frac{\partial \mathbf{B_0}}{\partial t} = \nabla \times (\mathbf{v_0} \times \mathbf{B_0}) + \lambda \nabla^2 \mathbf{B_0} + \nabla \times \langle \mathbf{v} \times \mathbf{b} \rangle \qquad (4)$$

$$\frac{\partial b}{\partial t} = \nabla \times (\mathbf{v_0} \times \mathbf{b}) + \nabla \times (\mathbf{v} \times \mathbf{B_0}) + \nabla \times \mathbf{G} + \lambda \nabla^2 \mathbf{b} \qquad (5)$$

where $G = \mathbf{v}\times\mathbf{b} - \langle \mathbf{v}\times\mathbf{b}\rangle$

The last term in (4) is the source of the fluctuation-induced electric field $E_F = -\langle \mathbf{v}\times\mathbf{b}\rangle \cdot \mathbf{B}/|\mathbf{B}|$ (using the normalization of Ch.3) which drives the RFP dynamo. The magnetic Lundquist number

$$S = \frac{\mu_0 v_0 a}{\eta} = \frac{\textit{flow velocity}}{\textit{magnetic diffusion velocty}}$$

is obtained from the ratio between the two terms on the right-hand sides of (3)[4] This method of dynamo drive, sometimes called the alpha effect, is "the heart of all modern dynamo theory"[5].

Assuming $\mathbf{b}(t=0)=0$, (5) implies a linear relationship between $\mathbf{b}$ and $\mathbf{B_0}$, therefore also between $\mathbf{B_0}$ and $\langle \mathbf{v}\times\mathbf{b}\rangle$. Then the dynamo term can be written as a rapidly convergent series

$$\varepsilon_i = \langle \mathbf{v}\times\mathbf{b}\rangle_i = \alpha_i B_{0j} + \beta_{ijk}\frac{\partial B_{0j}}{\partial r_k} + \gamma_{ijkl}\frac{\partial^2 B_{0j}}{\delta r_k \delta r_l} + \ldots \qquad (6)$$

where the coefficients depend on $\mathbf{V_0}$, $\mathbf{v}$ and λ. The leading term dominates when $\mathbf{B_0}$ is weakly nonuniform. When the velocity fluctuation field $\mathbf{v}$ "lacks reflectional symmetry" (or posesses vorticity $\omega=\nabla\times\mathbf{v}$), ε gives rise to a current $\mathbf{J} = \frac{\langle \mathbf{v}\times\mathbf{b}\rangle}{\eta} = \frac{\alpha \mathbf{B_0}}{\eta}$ parallel to the mean magnetic field. The mean helicity $\langle \mathbf{v}\times\omega\rangle$ in the velocity fluctuations distorts the magnetic field in a "cyclonic event"[6], twisting poloidal into toroidal field[7] as in Fig.A1.1.

Fig.A1.1a Fig.A1.1b

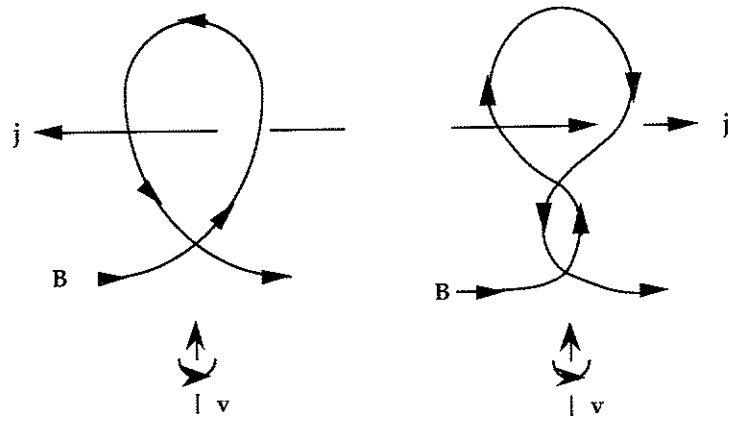

Field distortion by a localised helical disturbance (a 'cyclonic event').

In (a) the loop is twisted through an angle $\pi/2$ and the associated current is anti-parallel to **B**;
in (b) the twist is $3\pi/2$, and the associated current is parallel to **B**.

The field line twisting due to vorticity breaks the axisymmetry of the field. This permits solutions to the dynamo problem despite Cowling's "antidynamo" theorem[8], which implies that a reversed axisymmetric field is inconsistent with a steady-state plasma. Relaxation of the axisymmetry constraint by $\langle \mathbf{v}\times\mathbf{b}\rangle$ provides the means for steady-state field reversal: "Braginskii[9] demonstrated that, as Parker had argued,[10] non-axisymmetric motions could indeed provide an effective mean toroidal emf in the presence of a predominantly toroidal magnetic field."[11]

Reference

1 H.K. Moffatt, *Magnetic field generation in electrically conducting fluids,* Cambridge University Press 1978

2 ibid, p.145

3 R.B. White, in Handbook of Plasma Physics, Vol.1, edited by A.A. Galeev and R.N. Sudan (North-Holland, New York, 1983) 622

4 opcit, p.47

5 op cit, p.152

6 E.N. Parker, *The generation of magnetic fields in astrophysical bodies, I. The dynamo equations.* Astrophysical Journal **162** (1970) 665-73

7 op cit, p.153

8 T.G. Cowling, *The magnetic field of sunspots,* Mon. Not. Roy. Astr. Soc. **94** (1934) 39

9 S.I. Braginskii, *Self-excitation of a magnetic field during the motion of a highly conducting fluid,* Sov. Phys. JETP **20** (1964) 726

10 E.N. Parker, *Hydrodynamic dynamo models,* Ap. J. **122** (1955) 293

11 op cit, p.7

APPENDIX 2

REVIEW OF RESISTIVE TEARING MODES

Inclusion of resistivity and viscosity relaxes constraints on the ideal MHD equations, makes new states accessible to the plasma, and can result in higher growth rates.[1]. Viscous instabilities are not addressed here. The two most potentially dangerous resistive instabilities which have been recognized are resistive interchange modes and resistive tearing modes.[2,3] In both types of resistive instability, a mode of helicity (m,n) grows around its resonant surface, which lies at the radius r_s where the safety factor $q(r_s) = m/|n|$. Since resistive interchange modes are driven by pressure gradients one might expect them to be large in an RFP. However, these are stabilized by the RFP's high shear (q'/q), as evident in the criterion[4] for stability to resistive interchange modes:

$$\frac{r}{4}\left|\frac{\nabla q}{q}\right|^2 + \frac{2\mu_0 \nabla P}{B_z^2} > 0$$

and in the resistive interchange mode growth rate:[2]

$$\gamma \equiv \tau_R^{-1/3}\tau_A^{2/3}(kg)^{2/3}\left(\frac{\rho' q}{\rho q'}\right)^{2/3}$$

where $\tau_R \equiv a^2\mu/\eta$ is the resistive diffusion time, $\tau_A = \frac{a\sqrt{\mu_0\rho_0}}{B_0}$ is the Alfven time, k is the toroidal wavenumber, g is the gravitational acceleration, and ρ is the mass density.

The most virulent instability in the RFP is the resistive tearing mode, in which field lines tear and reconnect across a resonant surface. At r_s the (m,n) mode has the same pitch as the local magnetic field: the fluctuation amplitude is constant along the field line, so the mode's wavenumber parallel to the field vanishes. Transforming to a frame with zero shear at r_s, we see the field line from the point of view of the mode resonant at r_s, with[1]

$$\mathbf{B}_*(\mathbf{r}) = \mathbf{B}(\mathbf{r}) - \mathbf{B}(\mathbf{r})_{q=m/n} \qquad \text{where} \qquad \mathbf{B}(\mathbf{r})_{q=m/n} = \mathbf{B}_\theta(r_s)\, \mathbf{r}/r_s + \mathbf{B}_z(r_s)$$

In this frame, axial and poloidal fields vanish at the resonant surface:

Fig.A2.1

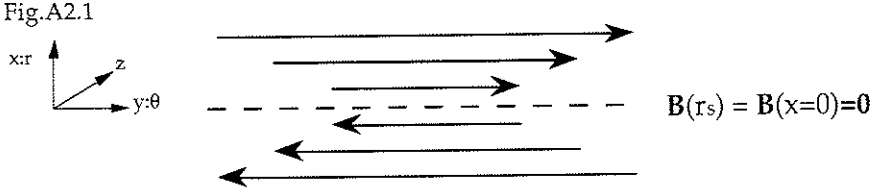

Since $B(r_s)=0$ in the frame of the perturbation, field lines can tear and reconnect into magnetic islands and a tearing mode instablity can grow at the resonant surface.[5] In a resistive plasma, a velocity perturbation gives rise to a current density perturbation $\mathbf{J}^1 = -\mathbf{v}\times\mathbf{B}/\eta$. This second-order current density crossed into the equilibrium magnetic field yields a restoring force opposed to the displacing flow:

Fig.A2.2

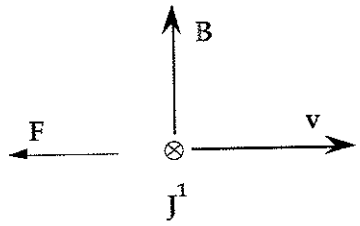

In a conducting fluid, the restoring force $\mathbf{J}^1\times\mathbf{B} = (\mathbf{v}\times\mathbf{B})\times\mathbf{B}/\eta \approx -\mathbf{v}B^2/\eta + (\mathbf{B}\cdot\mathbf{v})\mathbf{B}$ is infinite ($\eta\sim 0$) and the plasma is "frozen" to the magnetic field lines. With nonzero resistivity the magnetic restoring force against perturbations becomes finite.[6] Where B=0, the restoring force vanishes. The magnetic field lines can decouple from the plasma fluid, tear across the resonant magnetic flux surface, and reconnect into magnetic islands. For example, a radial magnetic field perturbation which varies poloidally can deform the plasma around the resonant surface .

Fig.A2.3

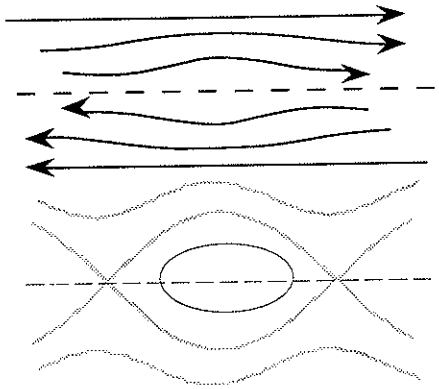

The perturbed flux surface can deform the plasma around the resonant surface, tear across r_s, and reconnect into magnetic islands. A (m,n) magnetic island is a helical filament of current which lies along the resonant surface, closing back on itself after m toroidal transits and n poloidal twists. Formation of magnetic islands reduces magnetic energy in the RFP,[6] therefore is favored in the presence of radial magnetic field perturbations across a resonant surface.

The perturbations associated with a magnetic island can be derived using a simplified slab model,[7] in which the radial direction is represented by x, the poloidal direction by y, and the axial direction by z. Assume cylindrical/axial symmetry ($\frac{\partial}{\partial z} \equiv 0$), incompressibility ($\nabla \cdot \mathbf{v} = 0$), and no mean flow ($\mathbf{V}$=0) or axial field perturbations (b_z=0). The radial magnetic field perturbation evolves according to Faraday's law:

$$(1) \qquad \frac{\partial b_x}{\partial t} = -\frac{\partial E_z}{\partial y}$$

where $E_z' = -v_x + \eta j_z$ and b, v, and j are perturbed quantities. Assuming sinusoidal variations in the poloidal direction, b_X~sin(ky) and v_Y~sin(ky), $\nabla \cdot \mathbf{B} = 0$ yields

$$(2) \qquad \frac{\partial b_x}{\partial x} = k b_y .$$

Incompressibility with axial symmetry yields $v_y = \frac{1}{k}\frac{\partial v_x}{\partial x}$. Taking the curl of B yields $j_z = \frac{1}{k}\frac{\partial^2 b_x}{\partial x^2} - k b_x$ so (1) becomes

$$(3) \qquad \frac{\partial b_x}{\partial t} = k v_x B_* - \eta\left(\frac{\partial^2 b_x}{\partial x^2} - k^2 b_x\right).$$

Away from the resonant surface (in the "fluid" region), the first term dominates, since resistivity η is small. Near the resonant surface (in the tearing region, or inside the "boundary layer"), the resistive terms dominate, since B_*~0. In this region, the velocity perturbations are vortices flowing toward the x-points and away from the o-point at the center of the separatrix, tending to widen the island radially, as in Figure A2.4 below:

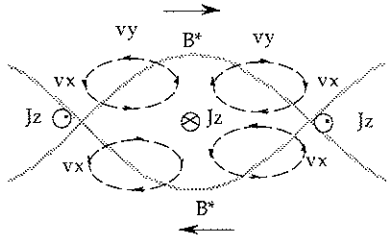

Axial current flows in a sinusoidal distribution on the resonant surface, out of the page at x points and oppositely directed at the island's center.

Solutions for the radial perturbation b_X are obtained in each region, then matched across the boundary layer, holding continuous.[2] Since the island current J_z is large only in the tearing region, it causes a discontinuity in ∇b_X, quantified by the logarithmic derivative, del-prime:

$$\Delta' = \frac{b_x'(r_{s+}) - b_x'(r_{s-})}{b_x(r_s)} = \frac{\partial}{\partial x}\ln(b_x(r_s))$$

where $b_x'(r_{s+})$ and $b_x'(r_{s-})$ indicate derivatives in the field perturbation at the outer edges of the island, and r_s corresponds to x=0 in the slab model of Fig.A2.1. [8]

The tearing mode growth rate γ and the magnetic island width ε can be obtained in terms of the logarithmic derivative Δ'. We find two equation in the two unknowns γ and ε, and solve for each in terms of Δ'. First we equate the rate at which the force $\rho\frac{\partial}{\partial t}v_x = -J_z B_*$ does work on the fluid:

$$v \cdot F \approx v_x B_* J_z \qquad (4)$$

with the rate of change of kinetic energy: $\frac{1}{2}\gamma\rho\left(v_x^2 + v_y^2\right) \cong \frac{1}{2}\gamma\rho v_x^2/(k\varepsilon)^2$. This yields

$$\gamma\rho v_x = 2B_* J_z (k\varepsilon)^2 \cong 2\Delta' B_* k\varepsilon b_x \qquad (5)$$

where we have approximated $\frac{\partial^2 b_x}{\partial x^2} \cong \frac{\Delta' b_x}{\varepsilon}$ in the boundary layer and $J_z \cong \Delta' b_z/k\varepsilon$ from the curl B equation. The second equation is obtained by assuming all three terms in Faraday's law are approximately the same size in the tearing region:

$$\gamma b_x \approx v_x k B_* \approx \eta k J_z, \text{ which reduces to } \lambda \approx \eta\Delta'/\varepsilon. \qquad (6)$$

Combining (5) and (6) yields the tearing layer width:

$$\varepsilon \equiv \left(\frac{\rho\eta^2\Delta'}{2(kB_*')}\right)^{1/5} \equiv S^{-2/5}(\Delta' a)^{1/5}\left(\frac{a}{R}n\frac{aq'}{q}\right)^{\pm 2/5}$$

and the resistive tearing mode growth rate:

$$\gamma \equiv .55\tau_R^{-3/5}\tau_A^{-2/5}(\Delta' a)^{4/5}\left(\frac{a}{R}n\frac{aq'}{q}\right)^{2/5}$$

(where $B_* \equiv B_*'\varepsilon$ has been used, and the factor .55 "comes from a more exact treatment"[6]). The tearing mode grows when the logarithmic derivative Δ' is positive (that is, when the slope of the perturbation increases across the boundary layer), and is stable when $\Delta'<0$.

Shear (q'/q) destabilizes the tearing mode, but several mechanisms contribute to the mode's saturation in a conducting-shell RFP. First, the v_y' flow which enlarges the island is opposed by a $J_z b_x$ force arising from a second-order current density $J_z \equiv v_y' b_x/\eta$. This force balances that in (4) when the island size $\sqrt{b_x/kB_*'}$ grows to the tearing mode width. Second, tearing modes quasilinearly modify the equilibrium profiles, flattening J and reducing the tearing mode driving term. Finally, nonlinear interactions between fluctuations result in a cascade of energy to shorter-wavelength ($m\geq 2$) modes, which serve as an energy sink and help stabilize the m=1 tearing mode fluctuations.[9]

References

1 Glenn Bateman, MHD Instabilities, The MIT Press, Cambridge Massachussetts, 1978

2 H.P. Furth, J. Killeen, M.N. Rosenbluth, Phys. Fluids **6** (1963) 459

3 B. Coppi, J.M. Greene, J.L. Johnson, Nuclear Fusion **6** (1966) 101

4 Suydam , Proc. 2d International Conference on Peaceful Uses of Atomic Energy **31** (1957) 157

5 J.M. Green and J.L. Johnson, Plasma Physics **10** (1968) 729

6 R.B. White, in Handbook of Plasma Physics, Vol.1, edited by A.A. Galeev and R.N. Sudan (North-Holland, New York, 1983)

7 P.H. Rutherford, Phys. Fluids **16** (1973) 1903

8 H.P. Furth, P.H. Rutherford, H. Selberg, Phys. Fluids **16** (1973) 1054

9 J.A. Holmes, B.A. Carreras, P.A. Diamond, V.E. Lynch, Phys. Fluids **31** (1988) 1166

APPENDIX 3

SUMMARY OF BOUNDARY CONDITIONS

The original version of the DEBS code[1] included boundary conditions for a conducting shell at the plasma edge, r=a. A modified[2] version of DEBS allowed removal of the conducting shell to a distance r>a, and placement of a resistive shell at r=a. Modifications made to DEBS for the purpose of this thesis embed conducting[3] or resistive coils of helicity (m,n) in the resistive shell at r=a, and permit plasma rotation. The boundary conditions for each case are summarized in this appendix.

All versions of DEBS calculate the magnetic field components B_r, B_θ, B_Z from the vector potential **A**, which is advanced subject to boundary conditions on **B** and on the applied electric field **E**. Two equations

$$\mathbf{B} = \nabla \times \mathbf{A}$$

$$d\mathbf{A}/dt = -\mathbf{E}$$

are solved simultaneously. The axial and poloidal components of **A** are solved at two adjacent radial points in a two by two matrix, and A_r is found separately. The coefficients of this matrix are determined by the radial location, geometry, and resistivity of the shells outside the plasma. Different boundary conditions on B are imposed by changing these coefficients.

A3.1 IDEAL BOUNDARY CONDITIONS

Under the original ideal boundary conditions, a perfectly conducting shell is included at r=a, the plasma edge. Since the component of the magnetic field perpendicular to a conductor vanishes, these boundary conditions constrain $B_r(a)=0$. Therefore, the axial and poloidal components of the vector potential can be found from

$$B_r = (\nabla \times \mathbf{A})_r = \frac{1}{r}\begin{vmatrix} \mathbf{r} & r\theta & \mathbf{z} \\ \partial/\partial r & \partial/\partial\theta & \partial/\partial z \\ A_r & A_\theta & A_z \end{vmatrix} = \frac{1}{r}\left(\frac{\partial A_z}{\partial\theta} - \frac{\partial A_\theta}{\partial z}\right) = 0.$$

Assuming perturbations of the form $f(r)e^{-i(m\theta + kz)}$ in Fourier space, we can linearize $\mathbf{B} = \nabla \times \mathbf{A}$:

$$B_r = ikA_\theta - \frac{im}{r}A_z \qquad (0)$$

The equations used to evolve A are solved in DEBS as:

$$\begin{pmatrix} gg_{11} & gg_{12} \\ gg_{21} & gg_{22} \end{pmatrix}\begin{pmatrix} A_{\theta nr} \\ A_{znr} \end{pmatrix} - \begin{pmatrix} hh_{11} & hh_{12} \\ hh_{21} & hh_{22} \end{pmatrix}\begin{pmatrix} A_{\theta nrm1} \\ A_{znrm1} \end{pmatrix} = \begin{pmatrix} fjj_1 \\ fjj_2 \end{pmatrix} \qquad (1)$$

The upper equation applies boundary conditions corresponding to $\mathbf{B}=\nabla\times\mathbf{A}$, while the lower equation applies boundary conditions corresponding to $d\mathbf{A}/dt = -\mathbf{E}$. The latter is not modified in the present work.

A3.2 NONIDEAL BOUNDARY CONDITIONS

A3.2.1 RESISTIVE SHELL AT r=a

Since tangential components of the magnetic field are continuous across the plasma boundary, relaxation of the conducting shell condition at r=a permits a nonzero Br at the plasma edge. The coefficients for evolution of the vector potential can be derived as follows, where drp is simply the radial grid size at the specified location. In general, drp may vary in DEBS, but in practice it is usually held constant. From (0), B changes as:

$$\frac{dB_r}{dt} = ik\frac{dA_\theta}{dt} - \frac{im}{r}\frac{dA_z}{dt} \qquad (2)$$

The jump condition

$$\left[\frac{\partial b_r}{\partial r}\right]_a = \left.\frac{\partial b_r}{\partial r}\right|_{a+} - \left.\frac{\partial b_r}{\partial r}\right|_{a-} = B_r|_a \frac{\partial}{\partial r} - \frac{\Delta B_r(a)}{\Delta r(a)}$$

enters the time derivative as $\frac{\partial b_r}{\partial t} = \frac{a}{\tau_s}\left[\frac{\partial b_r}{\partial r}\right]_a$, so (2) becomes:

$$\frac{\partial B_r}{\partial t} + \frac{\tau_R}{\tau_S}\left[\frac{dB_r}{dr}\right] = ik\left(\frac{\partial A_\theta}{\partial t} + \frac{\tau_R}{\tau_S}\left[\frac{dA_\theta}{dr}\right]\right) - \frac{im}{r}\left(\frac{\partial A_z}{\partial t} + \frac{\tau_R}{\tau_S}\left[\frac{dA_z}{dr}\right]\right) \qquad (3)$$

At the plasma-shell boundary, a=(r(nr)+r(nr-1))/2 , we find, writing the grid point (nr-1) as nrm1:

$$\frac{1}{2}\left(\frac{B_{r_{nr}}+B_{r_{nrm1}}}{\Delta t}+\frac{\tau_R}{\tau_S}\frac{B_{r_{nr}}-B_{r_{nrm1}}}{drp_{nrm1}}\right)= \qquad (4)$$

$$\frac{ik}{2}\left(\frac{A_{\theta_{nr}}+A_{\theta_{nrm1}}}{\Delta t}-\frac{\tau_R}{\tau_S}\frac{A_{\theta_{nr}}-A_{\theta_{nrm1}}}{drp_{nrm1}}\right)-\frac{im}{2r}\left(\frac{A_{z_{nr}}+A_{z_{nrm1}}}{\Delta t}-\frac{\tau_R}{\tau_S}\frac{A_{z_{nr}}-A_{z_{nrm1}}}{drp_{nrm1}}\right)$$

Grouping terms, we obtain forms for coefficients c_1, c_2, c_3, c_4, in terms of the time-step, space-step, and constants, where d/dr is calculated from the vacuum Bessel function solutions:

$$B_{r_{nr}}\frac{1}{2}\left(\frac{1}{\Delta t}+\frac{\tau_R}{\tau_S}\left(\frac{d}{dr}-\frac{1}{drp_{nrm1}}\right)\right)=c_3B_{r_{nr}} \qquad (5a)$$

$$B_{r_{nrm1}}\frac{1}{2}\left(\frac{1}{\Delta t}+\frac{\tau_R}{\tau_S}\frac{1}{drp_{nrm1}}\right)=c_4B_{r_{nrm1}} \qquad (5b)$$

$$A_{\theta_{nr}}\frac{ik}{2}\left(\frac{1}{\Delta t}-\frac{\tau_R}{\tau_S}\left(\frac{d}{dr}-\frac{1}{drp_{nrm1}}\right)\right)=ikc_1A_{\theta_{nr}} \qquad (5c)$$

$$A_{\theta_{nrm1}}\frac{ik}{2}\left(\frac{1}{\Delta t}-\frac{\tau_R}{\tau_S}\frac{1}{drp_{nrm1}}\right)=-ikc_2A_{\theta_{nrm1}} \qquad (5d)$$

$$-A_{z_{nr}}\frac{im}{2r}\left(\frac{1}{\Delta t}-\frac{\tau_R}{\tau_S}\left(\frac{d}{dr}-\frac{1}{drp_{nrm1}}\right)\right)=\frac{-im}{r_{nr}}c_1A_{z_{nr}} \qquad (5e)$$

$$-A_{z_{nrm1}}\frac{im}{2r}\left(\frac{1}{\Delta t}-\frac{\tau_R}{\tau_S}\frac{1}{drp_{nrm1}}\right)=\frac{-im}{r_{nr}}c_2A_{z_{nrm1}} \qquad (5f)$$

The resultant coefficients are inserted into the evolution matrix as: $gg_{11} = ik\,c_1$, $gg_{12} = -(im/r)\,c_1$, $hh_{11} = ik\,c_2$, $hh_{12} = (-im/r)\,c_2$., and $fjj_1 = c_3\,(B_r)_{nr} + c_4\,(B_r)_{nrm1}$

A3.2.2 PERFECTLY CONDUCTING HELICAL FEEDBACK COILS

To apply conducting boundary conditions on targeted modes (m,n), we solve for the coefficients which correspond to $B_r = 0 = -imA_z/r + ikA_\theta$. Equations (0) and (2) above simplify to:

$$0 = ikA_\theta - \frac{im}{r}A_z$$

$$0 = -\frac{i}{2}\left[kA_{\theta_{nr}} - \frac{m}{r_{nr}}A_{Z_{nr}} + kA_{\theta_{nrm1}} - \frac{m}{r_{nrm1}}A_{Z_{nrm1}}\right]$$

This yields coefficients for equations (5) of $gg_{11} = ik/2$, $gg_{12} = -(im/2r_{nrm1})$, $hh_{11} = -ik$, $hh_{12} = (im/2r)$, and $fjj_1 = 0$, which supersede the resistive shell coefficients only for targeted modes.

A3.2.3 RESISTIVE HELICAL COILS

To model the effect of imperfect feedback coils, we choose the form of coefficients derived from (5), substituting an effective time for the feedback coils τ_{fb} in place of the shell time τ_S. The term τ_{fb} represents not a circuit response time, but the effective soak-in time for a shell of resistivity η_{fb}.

A3.2.4 PLASMA/ISLAND ROTATION BOUNDARY CONDITIONS

All versions of DEBS calculate the boundary fluid velocity components v_r, v_θ, v_z from $\mathbf{v} = -\frac{\mathbf{E}\times\mathbf{B}}{SB^2}$, which is solved after advancing

A. Resistive shell modifications[2] with a nonzero axial E field include an adiabatic compression term for v_r. More recent modifications[4] permit imposition of nonzero v_z and v_θ for rotation of the shell at r=a, or equivalently, rigid rotation of the bulk plasma. This is accomplished by applying a specified $v_z(0,0)$ and $v_\theta(0,0)$ at r=a in the velocity advance, then including these velocities in the convective derivative term of (2) above.

$$(\frac{\partial}{\partial t} + v\cdot\nabla)b_r = \frac{\partial b_r}{\partial t} - i\frac{n}{R}v_z b_r - i\frac{m}{a}v_\theta b_r \qquad (6)$$

The resultant coefficients for the boundary conditions on b_r are (5) with

$2\,f_{jj}1 = -i\,(kv_z + mv_\theta/r)$, where the factor two is required for consistency with the averaging performed in (4). Rates of acceleration (spin up) are specified independently by increasing v_z and v_θ at each time-step, before they are used in the boundary condition.

Proposed[5] modifications would permit rotation of individual modes of helicity (m,n). This is accomplished by rotating helical coils at the edge. Ampere's law yields relations between tangential current densities and jumps in the magnetic field across a resistive shell of thickness Δ^s and a feedback coil of thickness Δ^c:

$$\frac{\partial b_z}{\partial r} = -J_\theta + \frac{\partial b_r}{\partial z} \;\rightarrow\; [b_z] = -J^s_\theta\Delta^s - J^s_\theta\Delta^c$$
$$\frac{\partial b_\theta}{\partial r} = J_z + \frac{\partial b_r}{\partial \theta} \;\rightarrow\; [b_\theta] = +J^s_z\Delta^s + J^c_z\Delta^c$$
$$\hat{r}\times[b_{tan}] = J^s\Delta^s + J^c\Delta^c \qquad (7)$$

where [ ] = $B(a_+)$ - $B(a_-)$ is the jump in B across r=a, from the vacuum region to the plasma region.

Assuming quantities vary as $f(r)e^{-i(k\cdot x)}$, we can find the jump condition for the radial magnetic field from the divergence:

$$\nabla\cdot\mathbf{b} = \left[\frac{\partial b_r}{\partial r}\right] - i\mathbf{k}\cdot[b_{tan}] \text{ where } \mathbf{k} = \frac{n}{R}\hat{z} + \frac{m}{a}\hat{\theta}$$

Feedback coils can induce mode rotation by adding a convective derivative term (6) to Faraday's equation:

$$\nabla\times E = \nabla\times\eta J^s = -(\frac{\partial}{\partial t} + v\cdot\nabla)b_r = -\frac{\partial b_r}{\partial t} + i\frac{n}{R}v_z b_r + i\frac{m}{a}v_\theta b_r \qquad (8)$$

To apply this condition to individual modes, we have to account for the interaction between feedback coil currents J^c and currents J^s which arise in the shell:

$$\nabla\times\eta^s\mathbf{J}^s = \eta^s\nabla\times\mathbf{J}^s(r)e^{-i\mathbf{k}\cdot x} = \eta^s(-i\mathbf{k}\times\mathbf{J}^s) = \eta^s(-i\mathbf{k}\times\left(\frac{\hat{r}\times[b_{tan}] - \mathbf{J}^c\Delta^c}{\Delta^s}\right) \qquad (9)$$

This relation can be rewritten in terms of jump conditions [ ] at the shell:

$$k\times(\hat{r}\times[b_{tan}]) = (k\cdot[b_{tan}])\hat{r} - (k\cdot\hat{r})[b_{tan}] = \frac{1}{i}\left[\frac{\partial b_r}{\partial r}\right]$$

with $\mathbf{k}_\perp = -\frac{n}{R}\hat{z} + \frac{m}{a}\hat{\theta}$ and $f = \sqrt{\left(\frac{m^2}{a^2} + \frac{n^2}{R^2}\right)}$ and $\mathbf{k}\times\mathbf{J}^c = \mathbf{k}\times(J^c\mathbf{k}_\perp) = J^c f$

Then (9) becomes simply $\nabla\times\eta J^s = \frac{\eta^s}{\Delta^s}\left(\left[\frac{\partial b_r}{\partial r}\right] + iJ^c f\right)$, which can be substituted into (8) to yield:

$$\frac{\partial b_r}{\partial t} - i\left(\frac{n}{R}v_z + \frac{m}{a}v_\theta\right)b_r = \frac{\eta^s}{\Delta^s}\left(\left[\frac{\partial b_r}{\partial r}\right] + iJ^c f\right)$$

which determines rotation boundary conditions on B.

References

1 D.D. Schnack,PhD Thesis, University of California/Livermore, Lawrence Livermore Laboratory publication UCRL-52399, 1978

2 Y.L. Ho, PhD Thesis, University of Wisconsin-Madison, DOE/ER/53212-131

3 E.J. Zita, S.C. Prager, Y.L.Ho, D.D. Schnack, accepted for publication in Nucl. Fusion (1992)

4 E.J. Zita, S.C. Prager, Y.L.Ho, D.D. Schnack, Bull. Intl. Sherwood Fusion Theory Conf., Santa Fe, NM (Apr.1992) 2C45

5 Y-L Ho, private communication